



# Mllt11 Regulates Migration and Neurite Outgrowth of Cortical Projection Neurons during Development

 Danielle Stanton-Turcotte,<sup>1</sup> Karolynn Hsu,<sup>1</sup> Samantha A. Moore,<sup>1</sup> Makiko Yamada,<sup>1</sup> James P. Fawcett,<sup>2</sup> and  Angelo Iulianella<sup>1</sup>

<sup>1</sup>Department of Medical Neuroscience, and Brain Repair Centre, Faculty of Medicine, Dalhousie University, Life Science Research Institute, Halifax, Nova Scotia B3H-4R2, Canada, and <sup>2</sup>Departments of Pharmacology, Surgery, and Brain Repair Centre, Faculty of Medicine, Dalhousie University, Life Science Research Institute, Halifax, Nova Scotia B3H-4R2, Canada

The formation of connections within the mammalian neocortex is highly regulated by both extracellular guidance mechanisms and intrinsic gene expression programs. There are two types of cortical projection neurons (CPNs): those that project locally and interhemispherically and those that project to subcerebral structures such as the thalamus, hindbrain, and spinal cord. The regulation of cortical projection morphologies is not yet fully understood at the molecular level. Here, we report a role for Mllt11 (Myeloid/Lymphoid or mixed-lineage leukemia; translocated to chromosome 11/ALL1 Fused Gene From Chromosome 1q) in the migration and neurite outgrowth of callosal projection neurons during mouse brain formation. We show that *Mllt11* expression is exclusive to developing neurons and is enriched in the developing cortical plate (CP) during the formation of the superficial cortical layers. In cultured primary cortical neurons, Mllt11 is detected in varicosities and growth cones as well as the soma. Using conditional loss-of-function and gain-of-function analysis we show that Mllt11 is required for neuritogenesis and proper migration of upper layer CPNs. Loss of *Mllt11* in the superficial cortex of male and female neonates leads to a severe reduction in fibers crossing the corpus callosum (CC), a progressive loss in the maintenance of upper layer projection neuron gene expression, and reduced complexity of dendritic arborization. Proteomic analysis revealed that Mllt11 associates with stabilized microtubules, and *Mllt11* loss affected microtubule staining in callosal axons. Taken together, our findings support a role for Mllt11 in promoting the formation of mature upper-layer neuron morphologies and connectivity in the cerebral cortex.

**Key words:** axonogenesis; callosal projection neurons; microtubules; Mllt11/Af1q; neuritogenesis; neurodevelopmental disorders

## Significance Statement

The regulation of cortical projection neuron (CPN) morphologies is an area of active investigation since the time of Cajal. Yet the molecular mechanisms of how the complex dendritic and axonal morphologies of projection neurons are formed remains incompletely understood. Although conditional mutagenesis analysis in the mouse, coupled with overexpression assays in the developing fetal brain, we show that a novel protein called Mllt11 is sufficient and necessary to regulate the dendritic and axonal characteristics of callosal projection neurons in the developing mammalian neocortex. Furthermore, we show that Mllt11 interacts with microtubules, likely accounting for its role in neuritogenesis.

Received Jan. 17, 2022; revised Mar. 13, 2022; accepted Mar. 30, 2022.

Author contributions: A.I. designed research; D.S.-T., K.H., S.A.M., and M.Y. performed research; D.S.-T., K.H., J.P.F., and A.I. analyzed data; D.S.-T. wrote the first draft of the paper; J.P.F. and A.I. edited the paper; D.S.-T. and A.I. wrote the paper.

A.I. lab was supported for this project by the Canadian Institutes of Health Research (CIHR) Grant PJT-388914. The J. P.F. lab was supported by a CIHR grant PJT-159738. We thank Sarah Whitehead, Emily Capaldo, Jessica Clark, and Di Shao for maintenance of mouse transgenic colonies and Marina Gertsenstein at the Center for Phenogenomics in Toronto, Canada, for assistance in generating chimeric mice. We also thank Leanne Clattenburg for advice on GST pull-down experiment.

M. Yamada's present address: Molecular Pharmacology Program, Memorial Sloan Kettering Cancer Center, New York, NY 10021.

The authors declare no competing financial interests.

Correspondence should be addressed to Angelo Iulianella at [angelo.iulianella@dal.ca](mailto:angelo.iulianella@dal.ca).

<https://doi.org/10.1523/JNEUROSCI.0124-22.2022>

Copyright © 2022 Stanton-Turcotte et al.

This is an open-access article distributed under the terms of the Creative Commons Attribution 4.0 International license, which permits unrestricted use, distribution and reproduction in any medium provided that the original work is properly attributed.

## Introduction

The mammalian neocortex is a complex structure, underlying the capacity for executive function, sensory processing, emotion, motor output, and cognition. Its laminated organization of excitatory pyramidal cortical projection neurons (CPNs) and inhibitory interneurons (INs) emerges from the coupling of neurogenesis with neuronal migration. Functional circuits emerge progressively during development as newborn neurons acquire molecular identities, dendritic morphologies, and projections characteristic of their laminar position. A fundamental question concerns how migration is controlled during sequential generation of more superficial cortical layers. While it is clear that the cytoskeleton plays a key role in neuronal translocation, its role in CPN subtype-specific neurite morphogenesis and the

maintenance of laminar transcriptional programs is not well understood. The sorting of differentiating CPN subtypes into discrete layers occurs as cells migrate radially from progenitor domains populating the ventricular zone (VZ) and adjacent subventricular zone (SVZ) along the apicobasal axis to invade the cortical plate (CP). The earliest-born CPNs migrate along radial glial fibers projecting from the basal surface of VZ progenitors to the pia via somal translocation as forces exerted on the cytoskeleton by motor proteins push and pull the nucleus toward the pia until a neuron reaches its terminal location (Bellion et al., 2005; Tsai et al., 2007). As the somas of these cells approach the pia, the trailing apical pole becomes the nascent axon projecting to form white matter (WM) tracts (Nadarajah et al., 2001; Marín and Rubenstein, 2003; Ayala et al., 2007; Sakakibara et al., 2014). Consequently, the intermediate zone (IZ) and CP become densely populated, necessitating multiple modes of motility in later-born upper layer (UL). These events rely on coordinated cytoskeletal reorganization as cells transiently acquire multipolarity to weave through the dense IZ and then reacquire bipolarity on invasion of the CP (Sakakibara et al., 2014). The growth of axons during brain formation also involves dynamic cytoskeletal reorganization at the growth cone in response to external guidance cues or cell-cell contacts (Hirokawa and Takemura, 2004; Ayala et al., 2007).

The ability to couple developmental cues with construction or degradation of microtubule networks underlie the propensity of CPNs to form connections intracortically and extracortically. As such, mutations of cytoskeletal components and interactors have been linked to various neurodevelopmental disorders that affect cortical formation, stabilization, and projections at the level of mitosis, axon guidance, disturbance of fasciculation of axonal tracts, or impaired migration (Moon and Wynshaw-Boris, 2013; Moffat et al., 2015).

While axonogenic mechanisms are conserved across CPN subtypes, the targeting and wiring of each cortical layer is dependent on its unique molecular characteristics. Each cortical layer expresses a unique transcription factor program that provides the molecular instructions for synapse formation with appropriate target regions of the brain. Beginning with the earliest-born Cajal–Retzius (CR) cells of layer 1 (L1), which secrete Reelin to guide the radial migration of nascent neurons (Frotscher, 1998; Chai et al., 2009, 2016; Gil-Sanz et al., 2013), neurogenesis and lamination proceeds in an inside-out, cross-repressive manner. Transcription factors Tbr1 (Hevner et al., 2001; Thomson, 2010) and Bcl11b/Ctip2 (Arlotta et al., 2005) of deep layer (DL)6 and DL5, respectively, suppress UL-specific factors until DL formation is complete and subcerebral projections are initiated (Toma et al., 2014). UL neurogenesis follows with expression of Satb2 in thalamically-targeted L4 CPNs (Hisaoka et al., 2010; Leone et al., 2015; Lopez-Bendito and Molnar, 2003), and co-expression of Satb2 (Alcamo et al., 2008; Britanova et al., 2008; Leone et al., 2015), Cux1 (CDP), and Cux2 (Nieto et al., 2004; Zimmer et al., 2004) in UL2/3 corticocortical CPNs, 80% of which project across the corpus callosum (CC; Leone et al., 2015).

In an effort to identify regulators of neural migration and differentiation, we previously reported the expression of Mllt11/Aflq (Myeloid/Lymphoid or mixed-lineage leukemia; translocated to chromosome 11/All1 Fused Gene From Chromosome 1q) in the developing CP (Yamada et al., 2014). Mllt11 is a

vertebrate-specific, 90 amino acid protein first identified as a fused protein with Mll in infant acute myeloid leukemia (Tse et al., 1995). Here, we report that Mllt11 is a neural-specific tubulin-associating protein and its inactivation in the superficial layers of the mouse brain results in improper migration and formation of callosal projections. Loss of *Mllt11* led to neurite outgrowth defects coupled with loss of UL-specific transcriptional programs characteristic of neurodevelopmental disorders. In contrast, *Mllt11* overexpression promoted the invasion of the CP by differentiating neurons. We provide evidence that Mllt11 interacts with stabilized microtubules, consistent with *Mllt11* mutants phenocopying brain tubulinopathies (Bahi-Buisson et al., 2014). Altogether, these findings contribute significantly to our understanding of the genetic regulation of CPN development, dendritic complexity, and axonal connectivity.

## Materials and Methods

### Animals

All animal experiments were done according to approved protocols from the IACUC at Dalhousie University. Mice (*Mus musculus*) carrying a null mutation in the *Mllt11* gene were generated using embryonic stem (ES) cell clones obtained from the mouse knock-out consortium project (UCDavis KOMP repository, *Mllt11tm1a(KOMP)Mbp/+*). The targeting construct is a “knock-out first, conditional second” approach, which inserts the gene encoding  $\beta$ -galactosidase ( $\beta$ -gal) into exon 2, the protein-coding sequence of the *Mllt11* gene. Two independently targeted clones were injected into blastocysts, and the resulting chimeras were mated to BL/6 females to achieve germ-line transmission. Offspring were genotyped by PCR using the following primers: wild-type forward (F) 5'-CGGTCCTGCCTTTGATTCTCAGC-3' and reverse (R) 5'-GCCTACTGCACAAGGTTCTTCTTGG-3' (expected product size: 379 bp), Mutant F 5'-GAGATGGCGCAACGCAATTAATG-3' and R 5'-AAGCAGTATTGCTTACTGGCCTGG-3' (expected product size: 274 bp). Heterozygotes (*Mllt11tm1a(KOMP)Mbp/+*) were maintained on a C57BL/6 background and crossed with *FlpO<sup>+/-</sup>* (B6.Cg-Tg(Pgk1-flpo)10Sykr/J, 011065, The Jackson Laboratory) mice and converted to a conditional allele via germ line Flp recombinase expression. Resulting *Mllt11<sup>Flox/Flox</sup>* offspring were crossed with *Ai9 Rosa26TdTomato* (B6.Cg-Gt(ROSA)26Sor<sup>tm9(CAG-tdTomato)Hze/J</sup>, 007909, The Jackson Laboratory) reporter line to generate *Mllt11<sup>Flox/Flox</sup>; Rosa26TdTomato<sup>+/-</sup>* or *Mllt11<sup>Flox/Flox</sup>; Rosa26TdTomato<sup>+/+</sup>* offspring.

*Cux2iresCre* mice used in this study to delete Mllt11 in developing UL neurons were previously described (Gil-Sanz et al., 2015; Yamada et al., 2015). *Cux2iresCre<sup>+/-</sup>* mice (B6(Cg)-*Cux2*<tm1.1(*cre*)Mull>/*Mmmh*, Mutant Mouse Resource and Research Center) were crossed with *Ai9 Rosa26TdTomato* (B6.Cg-Gt(ROSA)26Sor<sup>tm9(CAG-tdTomato)Hze/J</sup>, 007909, The Jackson Laboratory) mice. The resulting *Cux2iresCre<sup>+/-</sup>; Rosa26TdTomato<sup>+/-</sup>* or *Cux2iresCre<sup>+/-</sup>; Rosa26TdTomato<sup>+/+</sup>* offspring were crossed with the *Mllt11<sup>Flox/Flox</sup>; Rosa26TdTomato<sup>+/+</sup>* line to conditionally knock out Mllt11. Offspring of these crosses were genotyped using the following primers: wild-type F 5'-CGGTCCTGCCTTTGATTCTCAGC-3' and R 5'-GCCTACTGCACAAGGTTCTTCTTGG-3' (expected product size: 379 bp), Post Flp/Cre F 5'-CGGTCCTGCCTTTGATTCTCAGC-3' and R 5'-AAGCAGTATTGCTTACTGGCCTGG-3', and Cre F 5'-GTTATAAGCAATCCCCAGAAATG-3' and R 5'-GGCAGTAAAAA CTATCCAGCAA-3'. We genotyped for the presence of TdTomato using primers F 5'-TACGGCATGGACGAGCTGTACAAGTAA-3' and R 5'-CAGGCGAGCAGCCAAGGAAA-3' (expected product size: 500 bp) and allelism was determined with primers F 5'-TCAATGGG CGGGGTCGTT-3', R 5'-TTCTGGGAGTTCTCTGCTGCC-3', and R 5'-CGAGGCGGATCACAAGCAATA-3' (expected product size: 250 pb for wild-type and 300 pb for mutant). Similar numbers of control and *Mllt11* cKO mutant male and female mouse embryos and neonates were used in the analysis. No sex differences in *Mllt11* cKO mutant phenotype were observed in pilot studies. Statistical analysis (see below) was conducted on combined numbers of male and female offspring.

### GST protein expression, mass spectrometry, and immunoprecipitation

#### GST-tagged protein expression

The entire *Mllt11* sequence was cloned into pGEX-4T-2 vector for GST pull-down assays. BL21 competent cells (Sigma) were transformed with pGEX-4T-2 (GST) and pGEX-4T-2-MLLT11 (GST-MLLT11). Colonies were picked and incubated overnight in 2-ml 2xYT media with ampicillin at 37°C with shaking. The following day, overnight culture was added to 150-ml 2xYT media with ampicillin and incubated at 37°C with shaking until OD<sub>600</sub> reached 0.6. Protein expression was induced by adding IPTG (Invitrogen) to the culture to a final concentration of 0.1 mM and shaken at 28°C for ~4 h. Cells were pelleted by centrifugation and resuspended in 8-ml NP-40 lysis buffer (50 mM Tris, pH 8.0, 150 mM NaCl, and 1% NP-40) with protease inhibitor cocktail (Sigma). Cells were nutated at 4°C for 10 min, sonicated on ice (30 s on/30 s off, for 3 min total, level 6 intensity), and again nutated at 4°C for 10 min. Lysed cells were pelleted and supernatant collected (protein lysate).

#### Immobilization of GST or GST-MLLT11 bait protein

GST or GST-MLLT11 proteins were immobilized to Glutathione Sepharose 4B beads (Pierce). GST or GST-MLLT11 protein lysates were added to equilibrated 50% bead slurry and nutated at 4°C for ~3 h. Beads with immobilized protein were collected, washed, and resuspended in PBS to make a 50% slurry.

#### GST pull-downs and mass spectrometry

Whole embryonic mouse brains were harvested at embryonic day (E) 15.5 and lysed in NP-40 lysis buffer with protease inhibitor cocktail (Sigma). Whole-brain lysates from one embryo were added to either 6-μg GST or 6-μg GST-MLLT11 bead slurries and nutated overnight at 4°C. Beads with bound lysate were pelleted, washed, resuspended in sample buffer. Samples were heated for 15 min at 37°C and run on an SDS-PAGE gel, then stained with Coomassie Blue (Pierce). Bands were cut from the SDS-PAGE gel and processed by Dalhousie's Biological Mass Spectrometry Core Facility.

#### Co-immunoprecipitation (co-IP) and Western blottings

HEK293 cells were transfected with myc or myc-MLLT11 vectors using Lipofectamine 2000 (Invitrogen). Twenty-four hours later, cells were lysed on ice with Tris-HCl lysis buffer containing 50 mM Tris-HCl, pH 7.4, 150 mM NaCl, 1 mM EDTA, 1% Triton X-100, and protease inhibitor cocktail (Sigma). Lysed cells were collected, centrifuged, and supernatant used for co-IP. Anti-c-Myc Agarose resin (Pierce) was used, as per manufacturer's protocol, to co-immunoprecipitate myc or myc-MLLT11 and their binding partners. Proteins were eluted from the resin with 50 mM NaOH, neutralized with 1 M Tris, pH 9.5, and added to nonreducing sample buffer for Western blot analysis. For whole-brain lysates, E18.5 cortical protein samples were separated on 8% SDS-PAGE gels for 1 h at 120 V and transferred overnight at 20 V on to PVDF membranes (Bio-Rad). Blots were probed with mouse anti-acetylated tubulin (1:20,000, Sigma), and rabbit anti-Mllt11 (1:2000, Abcam). Secondary antibodies were goat anti-rabbit HRP (1:5000, Invitrogen) and goat anti-mouse HRP (1:5000, Invitrogen). Blots were developed with Clarity Western ECL Substrate (Bio-Rad) and imaged on a ChemiDoc Touch Gel Imaging System (Bio-Rad). Band densitometry was done using Image Lab Software (Bio-Rad).

#### qPCR

To confirm the loss of *Mllt11* transcripts, E18.5 RNA was extracted from cortices of three genotypic conditional knock-outs (cKOs) and four controls using the RNeasy Micro kit (QIAGEN). RNA was reverse transcribed to cDNA using the SuperScript II Reverse Transcriptase kit (Invitrogen). qPCRs were conducted using the SensiFAST SYBR No-ROX kit (Bioline) with the following primers for *Mllt11* and internal control GAPDH: *Mllt11* F 5'-GAACTGGATCTGTCCGAGCT-3' and R 5'-GCGCTCTCCAGAAGTTGAAG-3', GAPDH F 5'-ACCACAGTCCATGCCATCAC-3' and R 5'-TCCACCACCCTGTTGCTGTA-3' (Weng et al., 2014). Reactions were performed in triplicates.

### Histology

Fetal brains were dissected out and fixed in 4% paraformaldehyde (PFA) for 4–8 h, depending on embryonic stage, before being equilibrated in sucrose, embedded in Optimum Cutting Temperature (OCT) compound (Tissue-Tek), and cryosectioned at 12 μm. Cortex morphology was assessed by DAPI staining. β-Gal staining was performed on cryosectioned slides using the β-Gal Tissue Stain kit (Millipore). Immunohistochemistry was conducted on E14.5–E18.5 brains as described previously (Iulianella et al., 2008).

Immunohistochemistry was conducted using the following antibodies: rabbit anti-CDP/Cux1 (1:100; Santa Cruz), mouse anti-Satb2 (1:250; Abcam), rat anti-Bcl11b/Ctip2 (1:500; Abcam), rabbit anti-Tbr1 (1:200; Abcam), rabbit anti-Cleaved Caspase 3 (CC3; 1:500; Cell Signaling Technology), rabbit anti-Pax6 (1:500; Abcam), goat anti-Sox2 (1:200; Santa Cruz), rat anti-Tbr2 (1:200; eBioscience), mouse anti-neurofilament 2H3 (1:200; DSHB, University of Iowa), rabbit anti-Tuj1 (Tubb3; 1:1000, Biologend), and mouse anti-acetylated α-tubulin (1:1000, Sigma). Species-specific Alexa Fluor 488-, 568-, 594-, and/or 647-conjugated IgG (1:1500; Invitrogen) secondary antibodies were used to detect primary antibodies.

*In situ* hybridization was performed on 30-mm frozen sections obtained from E18.5, postnatal day (P)7, P14, P21, and P28 Control and cKO brains fixed overnight as previously described (Yamada et al., 2014) using an *Mllt11* riboprobe.

For EdU birth dating studies, dams were injected intraperitoneally with 30 mg/kg body weight of EdU (Invitrogen) at E14.5, E16.5, and E18.5 and killed at E14.5 or E18.5. Sections were immunostained using the Click-It kit according to the manufacturer's protocol (Invitrogen).

For Golgi stains, brains were harvested from mice at P28 and subjected to the FD Rapid GolgiStain kit (FD Neurotechnologies) as per manufacturer instructions. Crude sections were cut and mounted on slides with PermMount Mounting Medium (Fisher Scientific). Four brains were analyzed per genotype and 30 neurons per individual were analyzed.

#### Microscopy

Images were captured using a Zeiss AxioObserver fluorescence microscope equipped with an Apotome 2 structured illumination device, 10×, 20×, and a Hamamatsu Orca Flash v4.0 digital camera. β-Gal and *Mllt11 in situ* staining was captured using an upright Zeiss PrimoStar compound microscope with an ERc5s color camera. Images were processed using Zen software (Zeiss) and Photoshop CS6 (Adobe).

### Primary cortical cell culture and immunocytochemistry

Cortices were microdissected from E18.5 embryos, digested in trypsin (Pierce), manually triturated and plated on 35-mm well onto poly-D-lysine coated coverslips at a density of 150,000 cells for the neurite outgrowth assay or 500,000 for cellular localization experiments. Cells were plated in medium containing DMEM with 10% FBS and 1% penicillin/streptomycin and 4 h after plating, media was completely removed and replaced with Neurobasal media containing B-27+ (Gibco/Invitrogen), 1% penicillin/streptomycin, and L-glutamine. Cells were cultured for 24 h or one week in a 37°C incubator containing 5% CO<sub>2</sub>, then fixed for 10 min in 4% paraformaldehyde. Immunocytochemistry was conducted using the following antibodies: mouse anti-Tau (1:200; Abcam), rabbit anti-MAP2 (1:1000; Abcam), rabbit anti-Mllt11 (1:300, Abcam), rabbit anti-Tuj1 (Tubb3; 1:1000, Biologend), and mouse anti-acetylated α-tubulin (1:1000, Sigma).

### In utero electroporation and cDNA constructs

*In utero* electroporation was conducted using standard methodology under sterile surgical conditions (Saito, 2006). Endotoxin-free DNA was prepared according to the instructions of the manufacturer (QIAGEN) and injected at 1.5 μg/μl into the telencephalic vesicles of embryos in time-staged pregnant females anesthetized under inhalable isoflurane (5 l/min). A small incision was made on the ventral midline of anesthetized pregnant FVB females under a sterile field treatment. Single uteri containing the E13.5 fetuses were extruded and electric current was delivered across the fetal brains as five pulses for 50 ms at 900-ms



intervals using tweezer-style electrodes linked to the pulse generator CUY21 Vivo SQ (Sonidel). The embryos were returned in the body cavity, the peritoneum was sutured and the skin was stapled. Experimental plasmids used were *Mllt11-ires-eGFP*, and control plasmids included *pIRES2-EGFP* (Clontech) or pCIG (Addgene). To ensure comparable development staging, for each dam one uterus was electroporated with the experimental construct and the other with the control vector. Fetuses were allowed to survive for 2 d until E15.5 after which they were processed for cryosectioning to evaluate GFP expression and cortical layer development by immunostaining.  $N = 3$  *Mllt11-eGFP* and  $N = 4$  eGFP control fetal brains were analyzed.

### Dil tracing of callosal projections

Brains of E18.5 embryos were removed and embedded in 7% low gelling temperature agarose in DMEM medium with 1% penicillin/streptomycin. Embedded brains were crudely sectioned at a thickness of  $\sim 1$ – $2$  mm. Approximately  $0.5 \mu\text{l}$  of Dil (Invitrogen) was injected into the cortical WM tracts at rostral and caudal axial levels and incubated for 8 h in Tyrode's solution. Tissues were then fixed overnight at  $4^\circ\text{C}$  in 4% paraformaldehyde before incubating for two weeks at room temperature in PBS with 1% penicillin/streptomycin. Images were captured using a Zeiss V16 Axiozoom fluorescent stereomicroscope equipped with an AxioCam 506 mono digital camera (Zeiss).

### Image sampling, quantification, and analysis

For analysis of immunostaining markers and EdU, counting frames ( $100 \times 100 \mu\text{m}$ ) were placed in a vertical strip along the somatosensory (S1) cortex with the first counting frame along the edge of the ventricle. At least three histologic sections within the somatosensory cortex from three to eight different animals were analyzed for each immunostain, EdU or electroporated vector. Cells that were positively labeled for both DAPI and the marker were counted within each frame using ImageJ (FIJI; Schindelin et al., 2012). For analysis of primary cortical cell culture and Golgi stain, neurites were traced and measured and Sholl analyses were conducted using the "simple neurite tracer" plugin in FIJI. For analysis of radial glial parameters, E14.5, E16.5, and E18.5 cortical slices were immunostained with goat anti-Nestin antibodies (1:250, Santa Cruz). Control and *Mllt11* cKO mutant images were captured with identical acquisition parameters and radial glial morphology was assessed using the "directionality" plugin in FIJI to calculate the percentage of fibers in the image aligned in the same direction. Automatic thresholds were then applied and the area covered by Nestin staining was measured and expressed as a percentage of the total image area (Extended Data Fig. 3-1).

To ensure consistency among samples, cell counts were restricted to the presumptive S1 (somatosensory cortex) of the embryonic brain. In all experiments, three to six *Mllt11* KO and control embryos were used for quantification analysis using the unbiased and systematic sampling method we described previously (Yamada et al., 2015). Counts for *Ctip2*, *Tbr1*, *Cux1*, *Tbr2*, *Sox2*, *Pax6*, *CC3*, and *Satb2* are represented as line graphs, quantifying the proportion of DAPI stained cells expressing those markers. For EdU, TdTomato, and DAPI distribution analyses, proportion of total stained cells expressing markers within each cortical bin was quantified to ensure counting methods were consistent with previous studies (Chen et al., 2008; Lawrenson et al., 2017; Reyes et al., 2019). Image montages were assembled using Photoshop CS6.

### Statistical analysis

Statistical differences were determined with Student's *t* tests (two-tailed) with Welch's correction. Sholl analyses were performed with paired *t* tests (two-tailed) to compare branch points within comparable radii. Bar charts, line graphs, and statistical testing were conducted using GraphPad Prism V5.0d software, with results shown as mean  $\pm$  SD. In all quantification studies, significance level was set at  $p \leq 0.05$  (\* $p \leq 0.05$ , \*\* $p \leq 0.01$ , \*\*\* $p \leq 0.001$ , \*\*\*\* $p \leq 0.0001$ ).

## Results

### cKO of *Mllt11* from UL2/3 CPNs

*Mllt11* is expressed in developing neurons of the central nervous system, including the neocortex, but its role in cortical

neurogenesis is unknown (Yamada et al., 2014). To investigate the role of *Mllt11* in neurogenesis, we generated mice carrying a null mutation in the *Mllt11* gene using ES cell clones obtained from the mouse knock-out consortium project (UCDavis KOMP repository, *Mllt11*<sup>tm1a(KOMP)Mbp</sup>). We used the targeted (unflipped) allele to visualize *Mllt11* by  $\beta$ -galactosidase ( $\beta$ -gal) staining (Fig. 1A) because of the *LacZ* gene inserted into the *Mllt11* locus (Extended Data Fig. 1-1A). Initial *Mllt11* locus activity begins in the pallial MZ at E12.5, showing stronger expression in the IZ of the fetal cortex at E14.5 coinciding with the birth of basal progenitors fated to become UL2/3 CPNs, intensifying in the superficial cortical layers by E16.5–E18.5 (Fig. 1A). The localization of  $\beta$ -Gal staining reflected the activity of the *Mllt11* locus and confirmed our previous report of *Mllt11* mRNA and protein localization in differentiating neurons of the neocortex (Yamada et al., 2014). A detailed examination of *Mllt11* transcript expression by *in situ* hybridization revealed that cortical expression was maintained until P21, when it began to taper to levels indistinguishable from background at P28 (Extended Data Fig. 1-1B,C). In the hippocampus, *Mllt11* transcript levels decreased progressively from P7 to P21 and remained low at P28 (Extended Data Fig. 1-1C).

Given the temporal and spatial overlap between *Mllt11* expression and neurogenic regions of the cerebrum, we set out to investigate the role of *Mllt11* in the development cerebral cortex, and specifically in the formation of the UL2/3 callosally projecting CPNs that bridge communication interhemispherically (Fame et al., 2011) where *Mllt11* expression appeared highest during corticogenesis (Fig. 1A). We used a targeted *Mllt11* null allele to generate cKO *Mllt11* mice, in which the entire protein coding sequence in Exon 2 is flanked by loxP sites (Extended Data Fig. 1-1A). To avoid nonspecific effects of the selection cassette, mice encoding germline expressing flp recombinase were crossed to mice harboring the *Mllt11* targeted allele, leaving only loxP sites used to excise the entire protein-coding exon (exon 2) to create a conditional allele. Subsequently, to inactivate the *Mllt11* in UL2/3 of the cerebral cortex, we crossed the *Mllt11*<sup>Flox/Flox</sup> mice to the *Cux2iresCre* strain along with the *Ai9* TdTomato reporter mice to visualize recombined neurons, creating *Mllt11* cKO mutant (cKO) fetuses and neonates. *Cux2* is highly expressed in developing UL2/3 projections neurons, and mosaically expressed in the SVZ in the fetal pallial cortex (Nieto et al., 2004; Zimmer et al., 2004; Cubelos et al., 2008a,b). We confirmed *Mllt11* loss in UL CPNs by qPCR of E18.5 cortices (Extended Data Fig. 1-2A,B) as well as by ISH at P7 (Extended Data Fig. 1-2C,D) from *Cux2iresCre*-driven *Mllt11* cKO brains.

### Loss of *Mllt11* leads to a progressive decrease in cortical thickness

Brain and body weight did not differ significantly between *Mllt11* cKO mutants and controls at E18.5 (Fig. 1B–D). Mutants displayed a thinning of the cortex visible in the CP and WM beneath it (Figs. 1E, 5A,E). To explore the origin of this cortical thinning, we examined the morphology of the cortex beginning at E14.5 (Fig. 1F) when UL CPNs are born (Zimmer et al., 2004; Cubelos et al., 2008b). A thinning of the mutant cortex was observed beginning at E16.5 (Fig. 1G), increasing in severity by E18.5 (Fig. 1H). This was reflected by significant changes in the distribution of DAPI+ nuclei in deeper bins of the *Mllt11* cKOs, with a larger proportion of DAPI+ nuclei localized apically (toward the VZ) in E18.5 mutants relative to controls (Fig. 1H). We also evaluated whether programmed cell death could account for



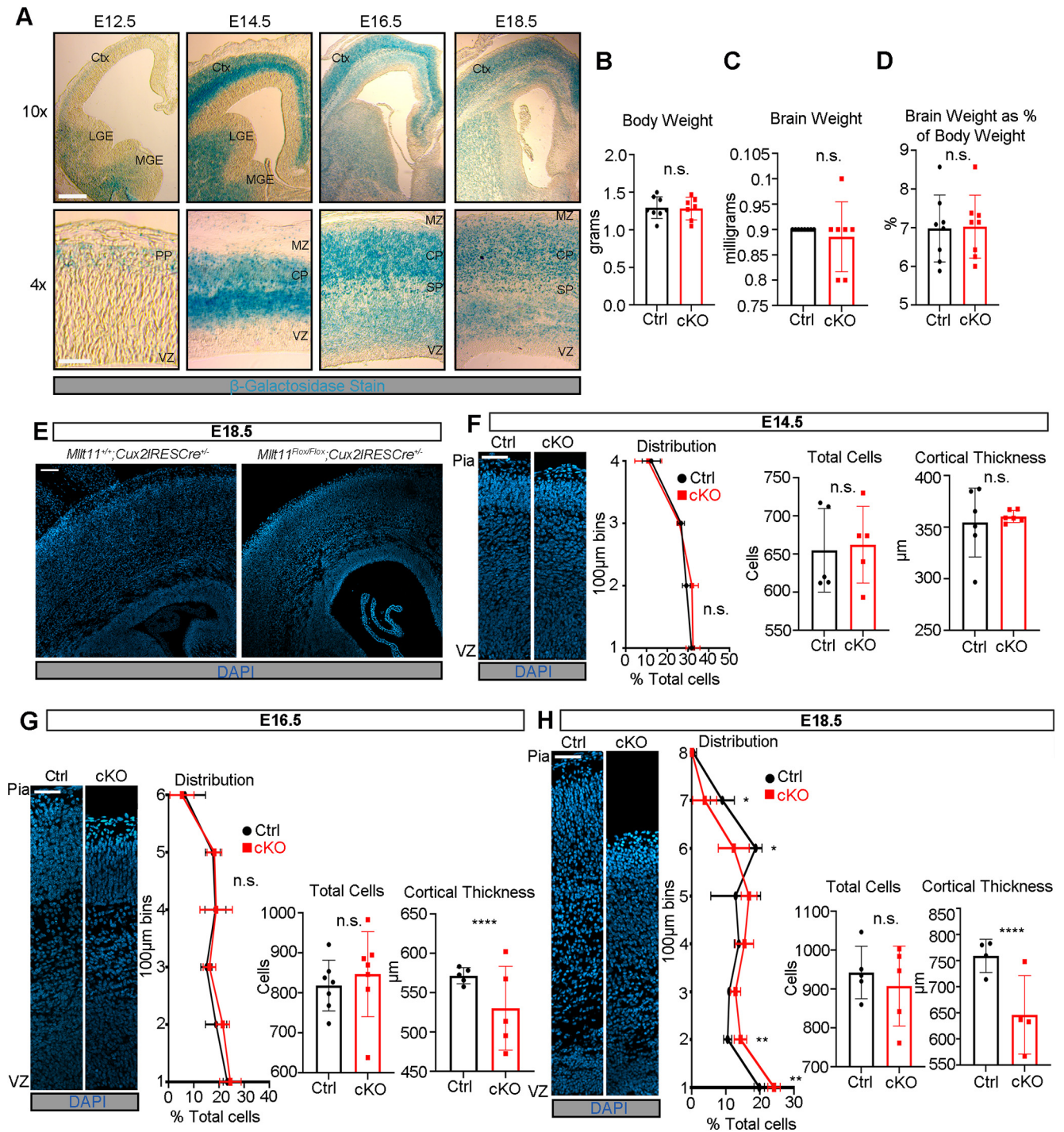


**Figure 1.** *Mllt11* is expressed in the developing CP and *Mllt11* loss affects the laminar distribution of cells. **A**, Coronal sections of the targeted *Mllt11* locus (which inserted a *lacZ* cDNA) showing *Mllt11* expression across four time points during cortical neurogenesis through  $\beta$ -Gal staining. At E14.5,  $\beta$ -Gal expression was most intense in the CP, corresponding to UL neurogenesis. By E16.5,  $\beta$ -Gal staining intensity shifted to the superficial cortex where UL CPNs were accumulating. **B–D**, Body weight (**B**), brain weight (**C**), and brain weight as a percentage of body weight (**D**) showed no difference between control (ctrl) and cKOs at E18.5. **E**, cKO cortices were thinner than controls at E18.5. **F–H**, Thinning of the cKO cortex was progressive, with thicknesses being comparable to controls at E14.5 (**F**), but *Mllt11* mutants exhibited reduced thickness and reduced distribution of cells in the superficial cortex at E16.5 (**G**), which increased in severity by E18.5 (**H**). Total cell counts and cortical thickness measurements ( $\mu\text{m}$ ) are shown as bar graphs. Cell count line charts represent percentage of positive cells normalized to DAPI+ nuclei per  $100 \times 100 \mu\text{m}$  bin. Student's *t* test with Welch's correction, (**B–D**)  $N = 8$ , (**F**)  $N = 5$ , (**G**)  $N = 7$  for total cells,  $N = 5$  for cortical thickness, (**H**)  $N = 5$  for total cells,  $N = 4$  for cortical thickness. Data presented as mean  $\pm$  SD. n.s., not significant; \* $p \leq 0.05$ , \*\* $p \leq 0.01$ , \*\*\* $p \leq 0.001$ , \*\*\*\* $p \leq 0.0001$ . Scale bars:  $100 \mu\text{m}$  (**A**),  $100 \mu\text{m}$  (**E**),  $50 \mu\text{m}$  (**F–H**). Ctx, cortex; CP, cortical plate; IZ, intermediate zone; LGE, lateral ganglionic eminence; MGE, medial ganglionic eminence; MZ, marginal zone; PP, preplate; SP, subplate; VZ, ventricular zone. See Extended Data Figures 1-1, 1-2, 1-3, 1-4, 1-5.

the cortical thinning, but did not find any cells positive for the apoptotic marker CC3 in the *Mllt11* cKO mutant neonatal cortex (Extended Data Fig. 1-3A,B), while retrosplenial regions, which typically show enhanced apoptosis, showed

similar CC3+ staining in both controls and mutants (Extended Data Fig. 1-3C).

*Mllt11* expression was restricted to the developing CP and not in the apical progenitor regions (VZ) of the cortex (Fig. 1A).

To rule out potential cell nonautonomous contributions from neural progenitors to the *Mllt11* mutant cortical phenotype we quantified cells positive for progenitor markers from E14.5 to E18.5, corresponding to the period of UL neurogenesis. Pax6, a radial glial cell (RGC) marker (Götz et al., 1998), was unaltered on *Mllt11* loss at all observed time points (Extended Data Figs. 1-4A–C, 1-5A–C). Sox2, a less restrictive marker for neural progenitors and quiescent RGCs (D'Amour and Gage, 2003; Ellis et al., 2004), also exhibited no significant differences in expression in the *Mllt11* cKO mutants compared with controls (Extended Data Figs. 1-4D–F, 1-5D–F). Tbr2<sup>+</sup> intermediate (basal) progenitors, which give rise to UL 2/3 CPNs, did not differ markedly between control and *Mllt11* cKO groups, but displayed fewer cells within deep (nonprogenitor) regions of the mutant cortex at E18.5, suggesting alterations in the formation and/or migration of nascent neurons from the SVZ (Extended Data Figs. 1-4G–I, 1-5G–I).

### *Mllt11* is required for the maintenance of UL CPN molecular identity

The transcriptional de-repression loop that specifies cell types in discrete cortical laminae coincides with the birth and migration of projection neurons (Kumamoto et al., 2013; Toma et al., 2014). Thus, a loss of *Mllt11* in UL progenitors can potentially affect neuronal birth, migration, and/or specification. We therefore investigated whether *Mllt11* loss had any role in regulating the molecular identity of UL CPNs. Expression of *Satb2* in CPNs of L2-4 exhibited a decrease at E18.5 (Fig. 2C; Extended Data Fig. 2-1C) as did *CDP/Cux1*, another marker of UL CPNs (Fig. 2F; Extended Data Fig. 2-1F). Investigation at earlier developmental time points revealed that this phenotype was progressive, beginning at E16.5 and increasing in severity by E18.5 (Fig. 2A,B,D,E; Extended Data Fig. 2-1A,B,D,E). While the extent of *CDP/Cux1* and *Satb2* staining displayed variability across individual mutants, there was a consistent decrease in expression levels an apical shift in expression domain in all *Mllt11* cKOs (Fig. 2C,F; Extended Data Fig. 2-1C,F). TdTomato labeling was used as a short-term lineage tracer of *Cux2*<sup>+</sup> intermediate progenitors that give rise to UL2/3 CPNs, and while TdTomato levels were largely unaltered at all time points (Fig. 2G–I), there was a consistent apical shift in expression domain at E18.5 (Fig. 2I). Collectively, these findings suggested that *Mllt11* loss in nascent UL neurons did not affect their neurogenesis, or the activation of UL gene expression programs, but may have affected their migration to contribute to L2/3 formation.

The cortical de-repression loop functions on a cellular level by alternately repressing DL and UL fate (Toma et al., 2014) so we wanted to determine whether the loss of UL CPN fate was coupled with a complementary upregulation of DL CPN fates in these cells. We examined the localization of DL6-specific and DL5-specific markers *Tbr1* and *Ctip2*, respectively, in *Mllt11* cKOs and controls at E14.5–E18.5 (Fig. 2J–O; Extended Data Fig. 2-1G–L). *Mllt11* cKO mutants displayed an apical shift in the expression domains of both *Tbr1* and *Ctip2* from E16.5 to E18.5, consistent with decreased cortical thickness and impaired UL formation (Fig. 2K–O; Extended Data Fig. 2-1H–L).

### *Mllt11* is required for the migration of UL CPNs

Given the thinning of the cortex and shift of cortical layer markers throughout development, we hypothesized that *Mllt11* may regulate CPN migration into the CP. To explore the role of *Mllt11* in CPN migration, we pulsed pregnant dams with EdU to label UL CPNs at E14 or E16 and observed the localization of EdU at E18.5. CPNs labeled with EdU at E14 exhibited an apical

shift of roughly 100  $\mu$ m in the *Mllt11* cKO mutants relative to controls (Fig. 3A), consistent with a decrease in cortical thickness in the cKOs (Figs. 1, 2). A greater proportion of E14-born CPNs remained restricted to the deeper bins of *Mllt11* cKO cortices relative to controls (Fig. 3A). As CPNs labeled with EdU at E16 were still in transit by E18, with only a few control CPNs reaching the outermost layers of the cortex, the discrepancy in UL cell migration was less pronounced in cKOs (Fig. 3B). To examine whether *Mllt11* loss affected the neurogenesis of UL neurons, we pulsed dams with EdU for 2 h at E14, which efficiently labeled nuclei within the basal progenitor region (Fig. 3C). We observed no difference in the numbers or distribution of EdU<sup>+</sup> nuclei in *Mllt11* mutants versus control cortices after a short pulse at E14 (Fig. 3C). To determine whether *Mllt11* loss caused a delay in the timing of UL neurogenesis, we repeated this short pulse at E18 when UL neurogenesis is nearly complete and noted no differences in EdU<sup>+</sup> cells in the superficial cortex of *Mllt11* mutant versus control brains (Fig. 3D). We did observe a slight increase of EdU<sup>+</sup> cells in the deepest 100- $\mu$ m bin of the *Mllt11* mutant cortex relative to controls, possibly reflecting aberrant migration of later born neurons (Fig. 3D). Overall, the EdU birth dating analysis suggested that *Mllt11* primarily regulates the migration, but not neurogenesis, of UL CPNs into the CP.

Guidance of migratory CPNs is dependent on the earliest born CR cells of L1, which secrete Reelin to attract and halt neuronal migration at the pial interface (Tueting et al., 1999; Hirota and Nakajima, 2017). However, there were no differences in the expression of CR markers *p73* or *Reelin* at E14.5 (Fig. 3E) or E18.5 (Fig. 3F) following *Mllt11* loss in UL progenitors and nascent neurons, suggesting that the apparent migration defect was not because of abrogated Reelin signaling. Additionally, *Mllt11* loss did not result in the perturbation of the radial glial scaffold on which migrating nascent neurons rely to reach their respective laminae, as evidenced by the comparable distribution of *Nestin*<sup>+</sup> radial glia fibers in the *Mllt11* cKO mutant and control fetal cortices (Extended Data Fig. 3-1A,E,I). We quantified the radial glial angle (Extended Data Fig. 3-1B,F,J), average area covered (Extended Data Fig. 3-1C,G,K), and dispersion of fibers (Extended Data Fig. 3-1D,H,L) at E14.5, E16.5, and E18.5, respectively, and found no significant differences between controls and cKOs. We conclude that the migratory defects in *Mllt11* mutant cortices were not likely caused by alterations in the radial glial scaffold.

Given the migration deficit in *Mllt11* mutants, we examined whether its overexpression in fetal brains is sufficient to promote migration to the superficial regions of the developing cortex. We used *in utero* electroporation to express a bicistronic vector containing *Mllt11* and *GFP* cDNAs, or control *GFP* vector alone, in wild-type mouse embryonic forebrains. We performed electroporations in anesthetized pregnant dams at E13.5, by injecting a DNA solution containing expression vectors unilaterally into forebrain ventricles, and analyzed the resulting fetal brains 2 d after at E15.5, when neurons are migrating into the CP. At E15.5, neurons from fetal brains overexpressing *Mllt11-GFP* localized to the CP, demarcated with *Tbr1* staining (Fig. 4A,D,E), while neurons from fetal brains electroporated with *GFP*-expressing control plasmids had yet to migrate out of the SVZ and IZ, identified by *Tbr2* staining (Fig. 4B–E). This experiment demonstrated that *Mllt11* overexpression is sufficient to promote migration into the developing CP. Taken together, our loss and gain-of-function analyses strongly support a cell autonomous role for *Mllt11* in promoting nascent UL neuronal migration in the developing CP.



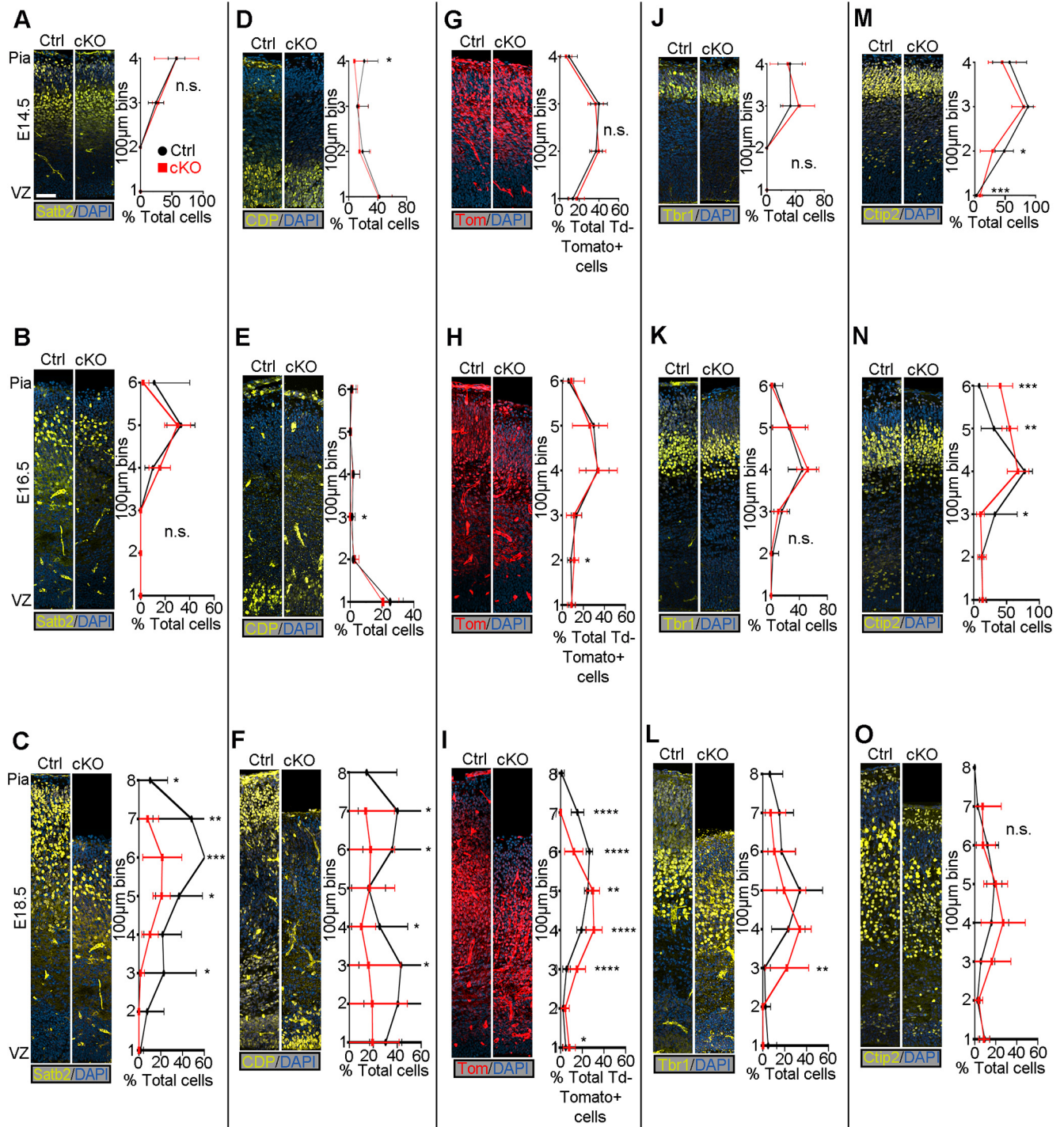


**Figure 2.** *Mllt11* loss progressively perturbed the formation of UL CPNs. **A–O**, Coronal cortical slices stained for cortical layer markers. **A, B**, Coronal cortical slices stained for *Satb2* expression were similar between *Mllt11* cKOs and controls at E14.5 (**A**) but displayed decreased numbers of *Satb2*+ cells in upper bins, and an apical shift at E16.5 (**B**). **C**, *Mllt11* cKO cortices displayed decreased *Satb2*+ cell numbers and apical shift at E18.5 compared with controls. **D, E**, *CDP/Cux1*+ cell numbers were largely normal at E14.5 (**D**), but began to decrease at E16.5 (**E**). **F**, *CDP/Cux1* levels were severely decreased in *Mllt11* cKOs compared with controls at E18.5. **G–I**, Distribution of *TdTomato* expression in the cortex was comparable between controls and cKOs at E14.5 (**G**), E16.5 (**H**), and E18.5 (**I**). **J–L**, *Tbr1* levels and localization were comparable between control and cKO at E14.5 (**J**) and E16.5 (**K**), but its expression domain exhibited an apical shift at E18.5 (**L**). **M–O**, *Ctjp2*+ cell numbers and localization were largely unaltered in cKO at E14.5 (**M**) and E16.5 (**N**) but exhibited an apical shift in expression domain at E18.5 (**O**). Line charts represent percentage of positive cells normalized to DAPI+ nuclei per 100 × 100 µm bin (**A–F, J–O**) and percentage of total *TdTomato*+ cells per 100 × 100 µm bin (**G–I**). Student's *t* test with Welch's correction, (**A, E, J, L–O**) *N* = 4, (**F–I**) *N* = 5, (**G**) *N* = 5 controls, 6 mutants, (**K**) *N* = 4 controls, 5 mutants. Data presented as mean ± SD. n.s., not significant; \**p* < 0.05, \*\**p* < 0.01, \*\*\**p* < 0.001, \*\*\*\**p* < 0.0001. Scale bar: 50 µm (**A–O**). VZ, ventricular zone. UL CPNs, upper layer cortical projection neurons. See Extended Data Figure 2-1.



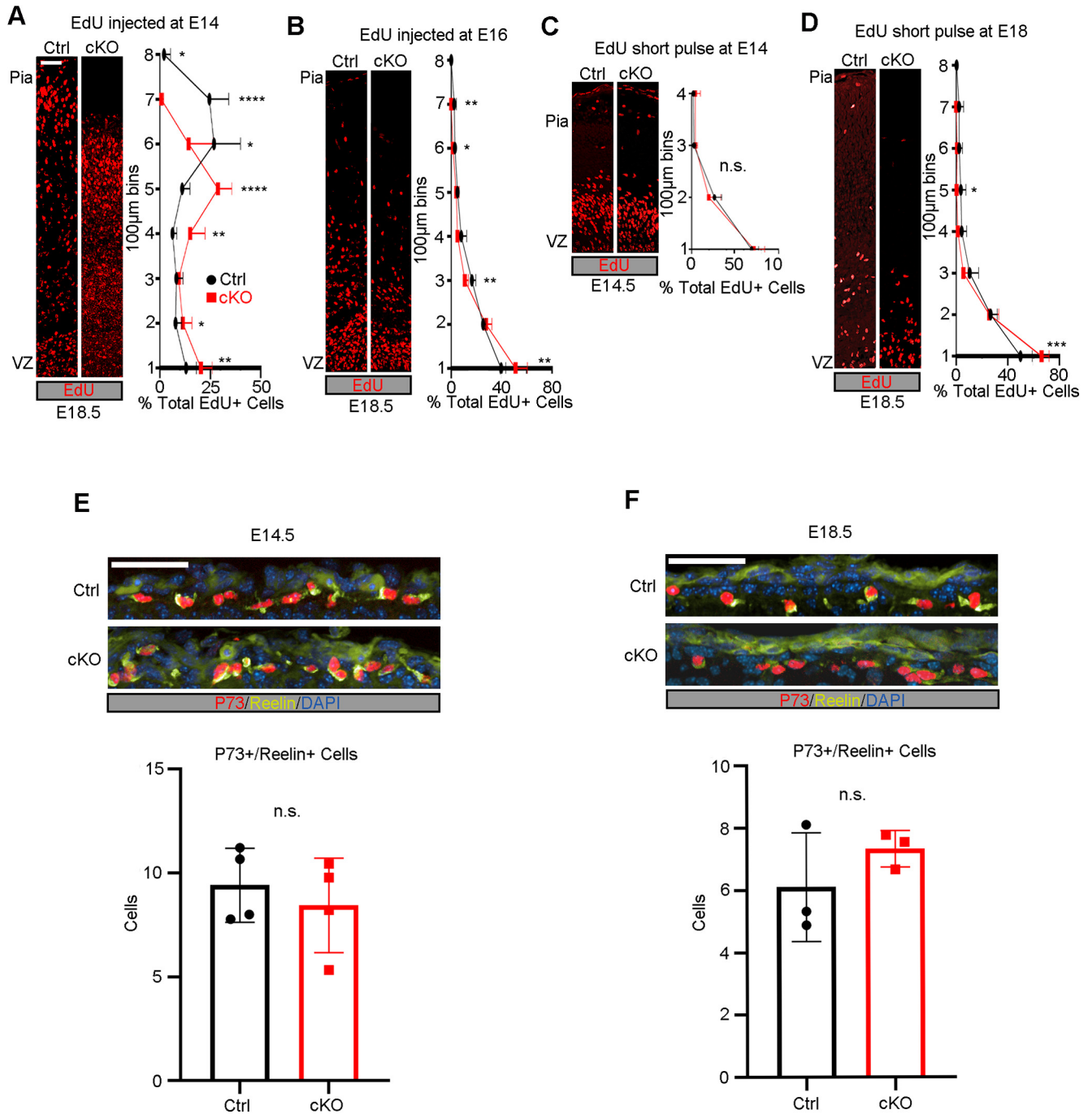


**Figure 3.** EdU birthdating demonstrated a CPN migratory defect in *Mllt11* cKO mutants. **A, B**, EdU birthdating of UL CPNs by injection at E14 showed altered distribution in *Mllt11* cKOs at E18.5, reflecting an apical shift in expression correlating with the decreased cortical thickness. **B**, Apical shift in migrating CPNs in cKOs relative to controls following an EdU pulse at E16 (**B**). **C**, Proliferating cells labeled with a short pulse of EdU at E14 showed no significant differences in numbers or distribution between controls and cKOs. **D**, No significant difference in numbers of nuclei labeled by a short pulse of EdU at E18 populating most bins in cKOs versus controls, but a greater proportion of cells were retained in the cKO VZ region. **E, F**, Pial sections at E14.5 (**E**) and E18.5 (**F**) showed comparable levels of expression of CR markers P73 and Reelin in L1 of cKOs versus controls. Line charts represent percentage of positive cells per 100 × 100 µm bin as a proportion of total EdU+ cells. Total co-labeled cells are shown as bar graphs. Student’s *t* test with Welch’s correction, (**A, C, E**) *N* = 4, (**B, D, F**) *N* = 3. Data presented as mean ± SD. n.s., not significant; \**p* ≤ 0.05, \*\**p* ≤ 0.01, \*\*\**p* ≤ 0.001, \*\*\*\**p* ≤ 0.0001. Scale bar: 50 µm (**A–F**). VZ, ventricular zone. CPN, cortical projection neuron. See Extended Data Figure 3-1.

***Mllt11* loss leads to reduced callosal crossing fibers and a thinning of WM tracts**

The migratory defects alone may be insufficient to explain the decreased cortical thickness of *Mllt11* cKO brains at E18.5 (Fig. 1*E,H*). Given that reduction in UL CPNs (Fig. 2*A,B*) would likely affect interhemispheric projections (Aboitiz and Montiel, 2003; Alcamo et al., 2008; Fame et al., 2011), we examined whether *Mllt11* loss impacted formation of projection fibers contributing

to the cortical WM tracts by staining for NF in coronal brain slices. We observed notable decreases in the thickness of NF+ fibers in the region of the fetal cortex containing WM tracts at E16.5 (Fig. 5*A–D*) and E18.5 (Fig. 5*E–H*) following *Mllt11* loss. Importantly, while NF+ fiber staining in the cc was greatly reduced in *Mllt11* cKOs at E18.5, NF+ fibers in the internal capsule, reflecting corticothalamic projections, remained unchanged in the mutant brains (Fig. 5*I*). Taken together, our findings

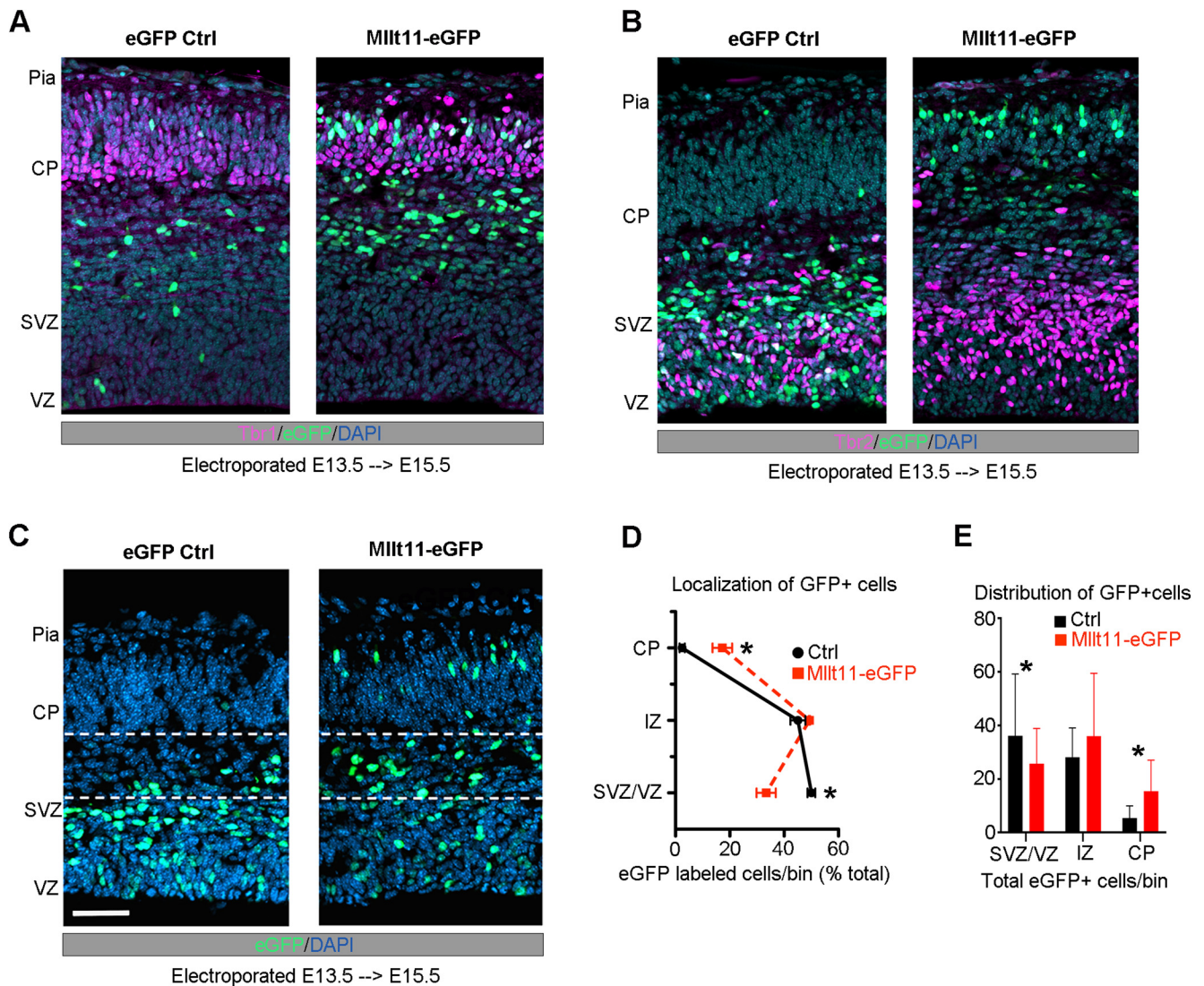


**Figure 4.** *Mllt11* overexpression promoted migration into the CP. **A, B**, E15.5 coronal cortical sections after electroporation at E13.5 with either a control eGFP (left) or *Mllt11-ires-eGFP* (*Mllt11*-eGFP) bicistronic plasmid (right). **B**, *Mllt11*-eGFP electroporation promoted migration into the CP, identified by Tbr1 staining. **C**, Control GFP (eGFP-control) electroporated cells remained mostly within the SVZ/VZ, identified by Tbr2 staining. **D, E**, Localization of eGFP-control and *Mllt11*-eGFP+ cells quantified as a percentage of total eGFP+ cells (**D**), and as the distribution of total eGFP+ cells per fetal cortical layer bin (**E**). Student's *t* test with Welch's correction;  $N = 3$  *Mllt11*-eGFP,  $N = 4$  eGFP controls. Data presented as mean  $\pm$  SD; \* $p \leq 0.05$ . Scale bar: 25  $\mu$ m (**A**). CP, cortical plate; IZ intermediate zone; SVZ, subventricular zone; VZ, ventricular zone.

revealed a critical role for *Mllt11* in UL CPN neurite morphology and axonogenesis of callosal fibers connecting the developing cerebral hemispheres.

The reduction of NF+ fibers crossing the cc in mutant brains suggested that *Mllt11* loss impacted the ability of UL2/3 CPNs to extend fibers across the telencephalic midline. To address the potential inability of *Mllt11* cKOs to extend axonal projections, we injected the lipophilic fluorescent dye DiI into the WM tracts of cortical slices at E18.5 and allowed it to diffuse through the tissue for two weeks before visualization. DiI labeling of projections was not detectable in the cc of *Mllt11* cKOs, while controls exhibited clearly labeled crossing callosal fibers (Fig. 5J). In contrast, the corticothalamic projections of the internal capsule were intact and traced by the DiI in both controls and cKOs, demonstrating that corticothalamic projections from DL6 were unaffected by the *Cux2iresCre* driven *Mllt11* cKO strategy (Fig. 5J). Altogether, our findings demonstrated that *Mllt11* loss in UL neurons specifically impacted the development of callosal projections.

### *Mllt11* interacts with cytoskeletal proteins

Our birthdating analysis suggested that the migratory defects observed in *Mllt11* cKOs are likely independent of the maintenance of UL transcriptional programs. To identify potential pathways through which *Mllt11* might be exerting its effects on CPN migration, we performed a GST pulldown assay to identify interacting proteins using lysate from E18.5 brains. Potential *Mllt11*-interacting proteins are listed in Table 1 and include multiple  $\alpha$  and  $\beta$  tubulin isoforms (>70% coverage) as well several atypical myosins, such as Myosin 5a (36%), Myosin 9 (24%), and Myosin 10 (8%). A potential association between *Mllt11* and tubulin is consistent with a recent whole cell proteomic study, which identified *Mllt11* as a likely interactor of both  $\alpha$ -tubulins and  $\beta$ -tubulins (Go et al., 2021). Given that acetylation of  $\alpha$ -tubulin is associated with stabilized microtubules and is crucial for outgrowth of stable neurites, we decided to focus on validating interactions between *Mllt11* and acetylated  $\alpha$ -tubulin by immunoprecipitation analysis. We overexpressed a myc-tagged *Mllt11* in Hek293 cells and pulled down acetylated- $\alpha$ -tubulin



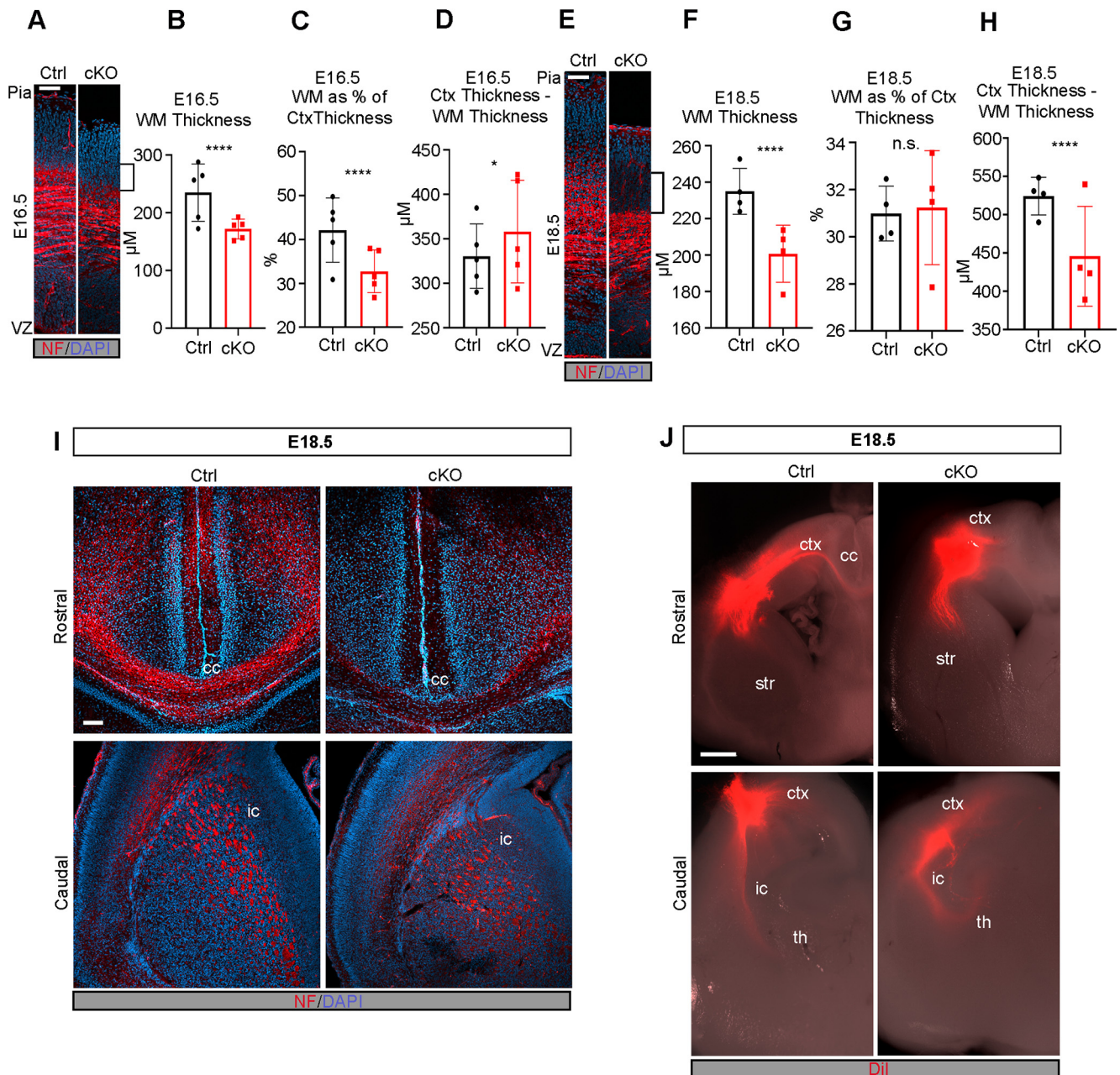


**Figure 5.** Formation of WM tracts and callosal projections is impaired in the *Mllt11* cKO cortex. **A**, Image of cortical WM tracts labeled with neurofilament at E16.5. Brackets indicate decreased WM. **B**, **C**, Quantification of cortical WM thickness (**B**) and WM thickness as a proportion of total cortical thickness (**C**) showed significant decrease in WM in cKOs relative to controls at E16.5. **D**, Quantification of cortical thickness subtracted from WM tract thickness showed a slight increase in *Mllt11* cKO mutants compared with controls at E16.5. **E**, Image of cortical WM tracts labeled with neurofilament at E18.5. Brackets show decreased WM staining area. **F–H**, Quantification of cortical WM thickness (**F**), WM thickness as a proportion of total cortical thickness (**G**), and cortical thickness subtracted from WM tract thickness (**H**) all showed significant decreases in *Mllt11* mutants compared with controls at E18.5. **I**, **J**, Coronal sections of E18.5 cortices at rostral (upper panels) and caudal (lower panels) axial levels labeled with neurofilament (**I**) or traced with Dil (**J**). **I**, Neurofilament labeling of the corpus callosum was significantly decreased in cKO compared with controls but labeling of the internal capsule was unaffected. **J**, Dil labeling was absent in the corpus callosum of cKO slices while control cortices displayed crossing fibers labeled by Dil. Rostrally, the internal capsule was traced comparably in control and cKO cortices. Student's *t* test with Welch's correction, (**A–D**)  $N = 5$ , (**E–H**)  $N = 4$ , (**J**)  $N = 3$ . Data presented as mean  $\pm$  SD; \*\*\*\* $p \leq 0.0001$ . Scale bar: 200  $\mu\text{m}$  (**A**) and 50  $\mu\text{m}$  (**B**). ctx, cortex; cc, corpus callosum; str, striatum; th, thalamus; ic, internal capsule; VZ, ventricular zone; WM, white matter.

(Fig. 6A). Probing the blots with anti-Mllt11 antibodies confirmed this interaction was dependent on heterologous Mllt11 expression in the cells (Fig. 6B), validating an association between Mllt11 and stabilized tubulin isoforms.

To evaluate whether Mllt11 localized to growing neurites, we used immunocytochemistry to probe the subcellular distribution of Mllt11, Tubb3, and acetylated  $\alpha$ -tubulin in cultures of primary fetal cortical neurons. Cortical neurons were extracted from wild-type embryos at E18.5 and cultured for 24 h or one week,

then immunostained to reveal the localization of Tubb3, acetylated  $\alpha$ -tubulin, and Mllt11. After 24 h *in vitro*, corresponding to the extension of a primary neurite, Mllt11/Tubb3 co-localized in discrete punctate patterns in varicosities along the distal portion of the developing neurite, as well as in the growth cone with limited overlap in the soma (Fig. 6C,c') After one week in culture, neurons displayed a more elaborate neurite arborization pattern and acetylated  $\alpha$ -tubulin and Mllt11 were both detected along proximal portion of neurite (Fig. 6D).



**Table 1. Potential *Mllt11*-interaction targets from GST pull-downs in E18.5 whole-brain lysates**

Band	Accession	Description	Sum PEP score	Coverage (%)	# Peptides	# PSMs	# AAs	MW (kDa)	Reference
7	D3Z4J3	Unconventional myosin-Va (Myo5a)	201.776	36	53	240	1855	215.4	
7	Q8VDD5	Myosin-9 (Myh9)	181.542	24	36	142	1960	226.2	
6	Q3UH59	Myosin-10 (Myh10)	31.272	8	10	22	2013	233.3	
5	P63017	Heat shock cognate 71-kDa protein OS = <i>Mus musculus</i> OX = 10090 GN = Hspa8 PE = 1 SV = 1	199.247	59	32	303	646	70.8	Li et al. (2014)
5	P38647	Stress-70 protein, mitochondrial (Hspa9)	20.395	12	6	12	679	73.4	
5	P20029	Endoplasmic reticulum chaperone BiP (Hspa5)	23.74	10	5	50	655	72.4	
5	Q3THK7	GMP synthase [glutamine-hydrolyzing] (Gmps)	8.67	5	3	6	693	76.7	
5	O08553	Dihydropyrimidinase-related protein 2 OS = <i>Mus musculus</i> OX = 10090 GN = Dpysl2 PE = 1 SV = 2	12.297	15	4	7	572	62.2	
4	Q9CWF2	Tubulin $\beta$ -2B chain (Tubb2b)	381.396	74	29	1338	445	49.9	
4	Q7TMM9	Tubulin $\beta$ -2A chain (Tubb2a)	380.755	74	29	1340	445	49.9	
4	P99024	Tubulin $\beta$ -5 chain (Tubb5)	369.155	74	29	1232	444	49.6	
4	P68372	Tubulin $\beta$ -4B chain (Tubb4b)	365.578	74	29	1153	445	49.8	
4	Q9ERD7	Tubulin $\beta$ -3 chain (Tubb3)	347.246	72	28	970	450	50.4	
4	Q9D6F9	Tubulin $\beta$ -4A chain (Tubb4a)	324.979	73	27	993	444	49.6	Go et al. (2021)
4	P68369	Tubulin $\alpha$ -1A chain (Tuba1a)	255.603	66	27	557	451	50.1	Go et al. (2021)
4	P05213	Tubulin $\alpha$ -1B chain (Tuba1b)	241.479	66	26	519	451	50.1	
4	Q922F4	Tubulin $\beta$ -6 chain (Tubb6)	176.166	40	17	444	447	50.1	
4	P10126	Elongation factor 1- $\alpha$ 1 (Eef1a1)	74.451	37	10	62	462	50.1	
4	A2AQ07	Tubulin $\beta$ -1 chain (Tubb1)	54.274	13	7	202	451	50.4	
4	Q9D8N0	Elongation factor 1- $\gamma$ (Eef1g)	27.863	20	6	14	437	50	
4	Q3UX10	Tubulin $\alpha$ chain-like 3 (Tuba3)	30.405	8	4	89	446	50	
3	Q9CWF2	Tubulin $\beta$ -2B chain (Tubb2b)	239.301	71	24	304	445	49.9	
3	P99024	Tubulin $\beta$ -5 chain (Tubb5)	214.778	71	24	324	444	49.6	
3	Q9D8N0	Elongation factor 1- $\gamma$ (Eef1g)	193.321	65	23	324	437	50	
3	P10126	Elongation factor 1- $\alpha$ 1 (Eef1a1)	202.141	56	21	542	462	50.1	
3	Q9ERD7	Tubulin $\beta$ -3 chain (Tubb3)	158.874	64	21	199	450	50.4	
3	P68369	Tubulin $\alpha$ -1A chain (Tuba1a)	188.056	64	20	177	451	50.1	Go et al. (2021)
3	P05213	Tubulin $\alpha$ -1B chain (Tuba1b)	178.724	64	20	169	451	50.1	
3	Q9D6F9	Tubulin $\beta$ -4A chain (Tubb4a)	170.961	54	19	253	444	49.6	Go et al. (2021)
3	P62631	Elongation factor 1- $\alpha$ 2 (Eef1a2)	50.614	28	9	259	463	50.4	
3	Q8BFR5	Elongation factor Tu, mitochondrial (Tufm)	39.656	32	9	28	452	49.5	
3	P60710	Actin, cytoplasmic 1 (Actb)	41.856	31	7	24	375	41.7	
3	P17182	$\alpha$ -Enolase (Eno1)	27.891	24	7	12	434	47.1	
3	P62737	Actin, aortic smooth muscle (Acta2)	24.601	16	5	16	377	42	
3	Q3UX10	Tubulin $\alpha$ chain-like 3 (Tuba3)	19.056	8	4	36	446	50	
3	P10637-3	Isoform Tau-B of Microtubule-associated protein tau (Mapt)	14.659	14	4	17	364	38.2	
2	Custom-P97783	Protein AF1q ( <i>Mllt11</i> )	298.867	89	35	1363	320	36.7	
2	P48758	Carbonyl reductase [NADPH] 1 (Cbr1)	185.195	77	21	576	277	30.6	
2	P62908	40S ribosomal protein S3 (Rps3)	85.426	70	17	171	243	26.7	
2	P68040	Receptor of activated protein C kinase 1 (Rack1)	34.523	25	7	20	317	35.1	
2	O70251	Elongation factor 1- $\beta$ (Eef1b)	16.545	24	4	9	225	24.7	
2	Q9D819	Inorganic pyrophosphatase (Ppa1)	10.238	15	3	6	289	32.6	
2	Q80XN0	D- $\beta$ -hydroxybutyrate dehydrogenase, mitochondrial (Bdh1)	8.871	9	2	4	343	38.3	
1	P97783	Protein AF1q ( <i>Mllt11</i> )	48.499	92	6	111	90	10	

*Mllt11* expression displayed a high degree of overlap with acetylated  $\alpha$ -tubulin and  $\beta$ -tubulin isoforms differentially over neurite development, consistent with a role in neurite development. We next evaluated microtubule levels in the CC of *Mllt11* mutants and found that both Tubb3 and acetylated  $\alpha$ -tubulin staining was reduced in cKOs at E18.5, reflecting reduced axonal targeting to the midline in the mutants (Fig. 6E).

### *Mllt11* is required for neurite outgrowth and extension

The relationship between stabilized and dynamic forms of tubulin has been shown to regulate the migratory potential of neurons and neurite extension because of the cycling of microtubule severing during outgrowth (Sudo and Baas, 2010; Lin and Smith, 2015; Wei et al., 2018). If *Mllt11* loss affected the relative amounts of stabilized microtubules, we would expect to see significant changes in neurite morphogenesis of UL neurons. We

therefore evaluated the morphology of cultured primary cortical neurons from *Mllt11* cKO mutants. We took advantage of the Ai9 tdTomato+ reporter introduced into the *Cux2iresCre/+; Mllt11<sup>Flox/+</sup>* conditional mouse to efficiently label and isolate UL primary neurons in culture. After 24 h *in vitro*, the length of MAP2+ primary neurites was reduced in cKOs compared with controls (Fig. 7A,B), as was the total length of all neurites (Fig. 7C). Moreover, the proportion of total length of extended neurites represented by the primary neurite at 24 h was slightly increased in cKOs (Fig. 7D). Quantification of the average number of neurites per neuron revealed a significant decrease in cKOs compared with controls (Fig. 7E,F), further suggesting that initiation of neurite outgrowth was abrogated on *Mllt11* loss.

After one week of culture *in vitro*, the total neurite length was drastically reduced in *Mllt11* cKO CPNs (Fig. 7G). Since *Mllt11* loss progressively attenuated primary neurite outgrowth in

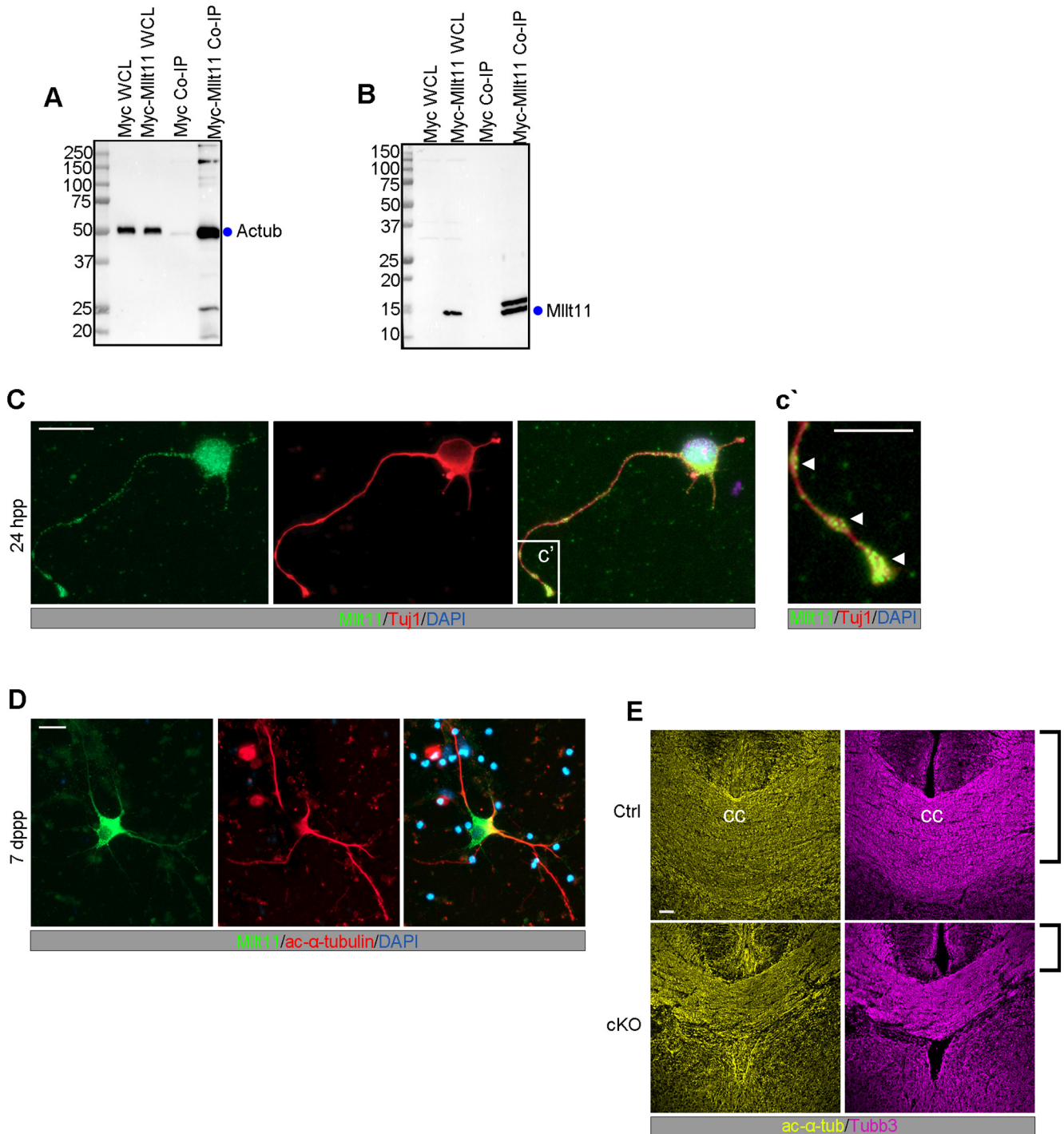


**Figure 6.** Mllt11 associated and colocalized with acetylated  $\alpha$ -tubulin in growing neurites. **A**, Co-IP of acetylated  $\alpha$ -tubulin (Actub) with Myc-tagged Mllt11 in whole cell lysates of HEK293 cells compared with a myc programmed control. **B**, Co-IP probed with Mllt11 antibody showing IP signal restricted to lanes containing Mllt11. **C, D**, Primary cortical neurons cultured for 24 h (**C**) or 7 d (**D**) postplating. **C**, After 24 h, Mllt11 colocalizes with Tubb3 in the growth cone and at swellings along the distal axon as indicated by arrowheads (**C'**), and in the soma (**C**). After 7 d, Mllt11 was primarily found along proximal portions of the axon where it colocalizes with acetylated  $\alpha$ -tubulin (**D**). **E**, Coronal sections of the corpus callosum (cc) at E18.5 labeled with acetylated  $\alpha$ -tubulin and Tubb3. Brackets show decreased thickness in cKO compared with control. Student's *t* test with Welch's correction, (**A, B**)  $N = 4$  (controls and cKOs). Data presented as mean  $\pm$  SD n.s., not significant (i.e.,  $p > 0.05$ ). Scale bar: 20  $\mu$ m (**C, D**) and 50  $\mu$ m (**E**).

cultured primary UL CPNs, we next evaluated a requirement for Mllt11 in the elaboration of dendritic arborization patterns in cultured CPNs. An advantage of using cultured neurons is that they are free of apical and basal contacts, allowing their neurites to radiate uniformly from the soma. This feature of two-dimensional neuronal culture allows for the evaluation of dendritic complexity by Sholl analysis. *Mllt11* mutant primary neurons

displayed much less complexity in the branching of their neurites (Fig. 7H,I), thus *Mllt11* loss greatly impacted the arborization patterns of cultured UL CPNs.

Given the prevalence of neurite growth and pruning during postnatal development, we evaluated the requirement of Mllt11 in the formation of dendritic arborization morphology characteristic of UL CNs *in vivo* at a time when mature

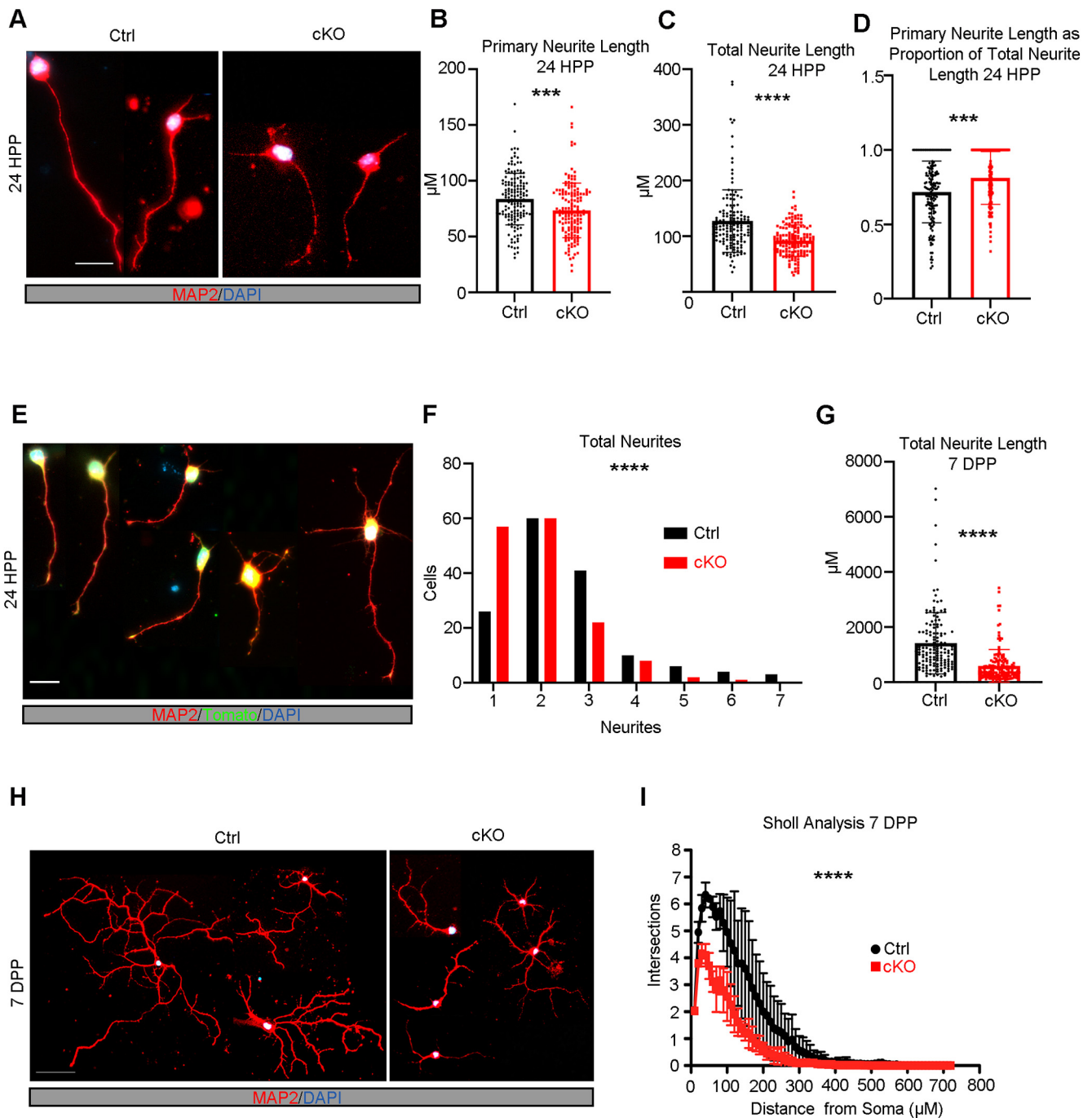


**Figure 7.** *Mllt11* loss decreased neurite outgrowth and branching complexity *in vitro*. **A**, Primary cortical neurons derived from E18.5 brains cultured for 24 h postplating. Neurites identified with MAP2 staining (red). **B**, **C**, Twenty-four hours postplating, primary neurite length (**B**) and total neurite length (**C**) were significantly decreased in cKO neurons relative to controls (**D**). The proportion of total primary neurite length was significantly increased in cKO neurons relative to controls. **E**, Examples of neuronal morphologies with varying numbers of neurites 24 h postplating. **F**, Quantification of number of neurites per neuron 24 h postplating, where cKO neurons had significantly fewer neurites compared with controls. **G–I**, Quantification of decreases in total neurite length (**G**) and branching complexity (**I**) of cKO relative to control primary cortical neurons cultured for 7 d postplating (**H**). Student's *t* test with Welch's correction (**B–D**, **F**). Paired *t* test, for both controls and cKOs  $N = 150$  neurons (50 neurons/individual  $\times$  three individuals). Data presented as mean  $\pm$  SD; \* $p \leq 0.05$ , \*\* $p \leq 0.01$ , \*\*\* $p \leq 0.001$ , \*\*\*\* $p \leq 0.0001$ . Scale bar: 20  $\mu\text{m}$  (**A**, **E**) and 50  $\mu\text{m}$  (**H**). HPP, hours postplating; DPP, days postplating.

arborization patterns have fully developed. Golgi staining was performed on control and *Mllt11* cKO brains harvested at P28 to capture mature CPN morphologies using the Golgi staining method. While control UL CPNs displayed complex dendritic morphologies typical of cortical pyramidal neurons (Fig. 8Aa–Ad), *Mllt11* cKOs UL CPNs displayed greatly attenuated dendritic arborization morphologies (Fig. 8Aa'–Ad'). We quantified the length of neurites in the Golgi-stained UL

CPNs of cKO and control brains and observed a severe decrease in total neurite length in the *Mllt11* mutants (Fig. 8B). The extent of decrease of neurite arborization *in vivo* was similar to that observed in cultured primary neurons (Fig. 7G–I). Sholl analysis revealed that the overall neuronal morphology was also much less complex with less elaborately-branched neurites in *Mllt11* cKO UL CPNs (Fig. 8C). Taken together, these findings confirmed a critical requirement of *Mllt11* in the growth and elaboration of



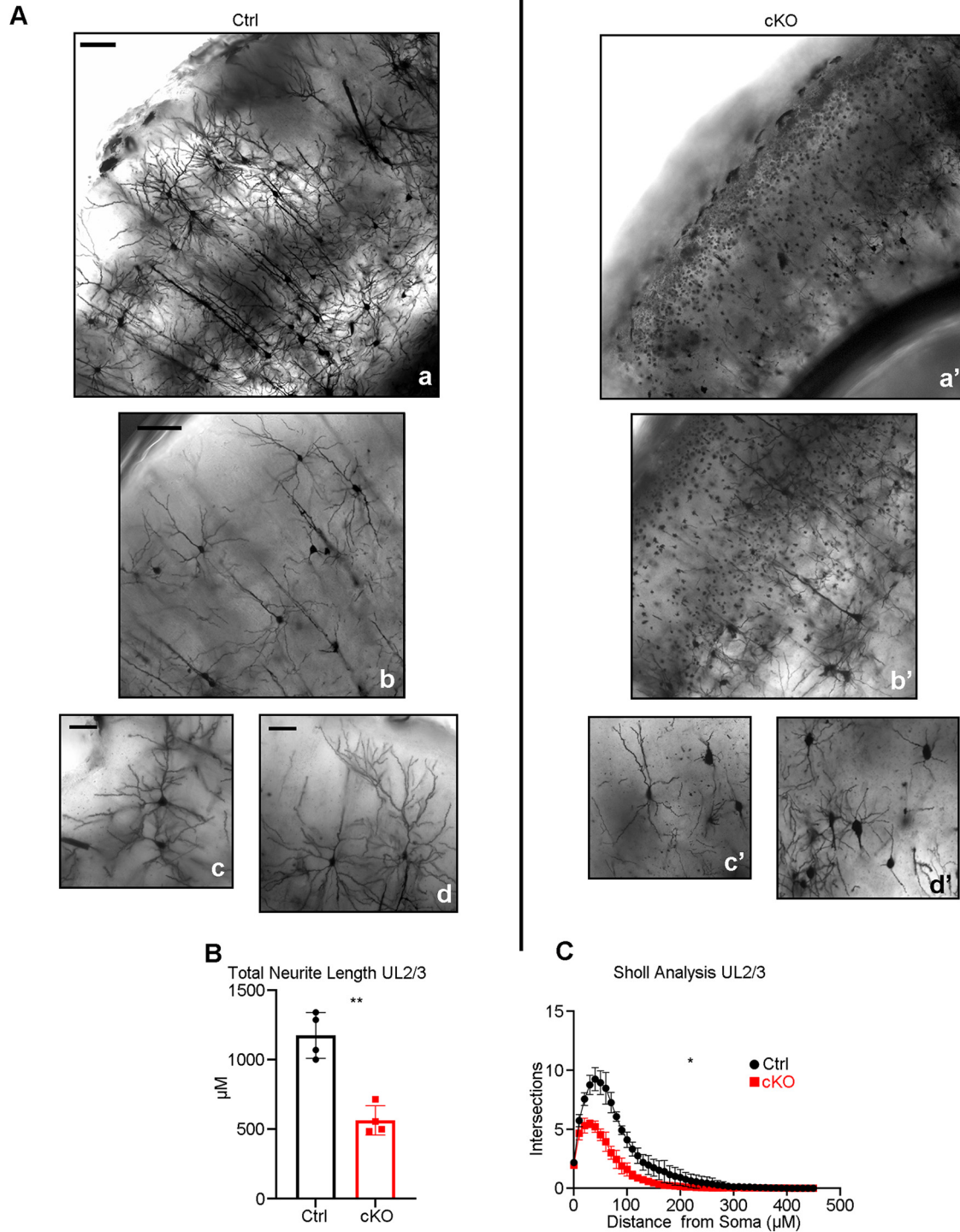


**Figure 8.** Decreased neurite outgrowth and branching complexity in UL CPNs in the *Mllt11* cKO cortex. **A**, Corresponding 100× (**Aa–Ad**) and 200× (**Aa'–Ad'**) magnification images of coronal sections of P28 Golgi-stained control (**Aa–Ad**) and *Mllt11* cKO cortices (**Aa'–Ad'**). **B, C**, Quantification of neurite length (**B**) and branching complexity (**C**) within UL2/3 showed reduced neurite length and branching complexity in cKOs compared with controls. Length measurements analyzed with Student’s *t* test with Welch’s correction, layer-specific Sholl analysis compared with paired *t* test, *N* = 4 (controls and cKOs), 30 neurons/individual. Data presented as mean ± SD; \**p* ≤ 0.05, \*\**p* ≤ 0.01. Scale bar: 100 μm (**Aa, Aa'**) and 50 μm (**Ab–Ad'**).

neurites during the development of mature superficial CPN morphologies and projection phenotypes.

**Discussion**

We described the role of a novel vertebrate-specific and neurologically restricted protein, Mllt11, in the regulation of neurite

extension and migration of superficial CPNs. The *Mllt11* locus has been identified in human genomic regions potentially affected in schizophrenia patients (Brzustowicz et al., 2002, 2004; Su et al., 2017), suggesting a role in CNS development. Our study is the first to demonstrate that Mllt11 regulates key aspects of cortical neuron morphogenesis and connectivity. Using the

*Cux2iresCre* driver to excise *Mllt11* in developing UL CPNs, we revealed that conditional *Mllt11* loss decreased cortical WM tracts and callosal fibers, and abrogated extension and maintenance of mature arborescent dendrites. Furthermore, *Mllt11* conditional mutants did not affect the formation of Reelin+ CR cells nor radial glial scaffolding, both of which are crucial for guiding the migration of CPNs. This suggests that *Mllt11* loss acted cell autonomously to hinder radial migration of CPN progenitors into the CP. The inefficient migration of UL CPNs in *Mllt11* mutant brains likely reflected a role for *Mllt11* in regulating the cytoskeleton, as it associated with stabilized microtubules, and was required for their maintenance in growing neurites. Neurons lacking *Mllt11* displayed deficits in neurite complexity both *in vivo* and *in vitro*, demonstrating that *Mllt11* is a critical regulator of neurite outgrowth.

We show that *Mllt11* interacts with tubulin isoforms, confirming a recent proteomic screen (Go et al., 2021), which provides a molecular rationale for the basis of the *Mllt11* mutant phenotype. Cortical thinning and increased ventricular lumen surface area are common phenotypes associated with neurodevelopmental disorders, and were observed in *Mllt11* mutant brains, suggesting cytoskeletal dysregulation may underlie a subset of these disorders (Bahi-Buisson et al., 2014; Mensen et al., 2017; Li et al., 2019). Moreover, changes in microtubule dynamics can affect neuronal migration and the generation of functional connections in the brain. These are processes whose dysfunction may underlie a wide spectrum of neurodevelopmental disorders. Given that *Mllt11* mutant mice displayed both migratory and neurite outgrowth defects, they are a model to study brain disorders arising from aberrant regulation of the neuronal cytoskeleton during development.

The microtubule cytoskeleton generates polarized force and provides a functional railway along which motor proteins migrate, whether to drive actin polymerization in generating protrusive forces at the leading edge of the growth cone, or integrate extracellular cues into regulation of microtubule activity (Dent and Kalil, 2001; Buck and Zheng, 2002; Lee et al., 2004; Zhou et al., 2004). Tubulin mutations have been shown to impair neuronal migration into the cortex (Aiken et al., 2017), and specifically affect UL CPNs (Keays et al., 2007) reliant on dynamic, multipolar cytoskeletal reorganization to extend short processes, “crawling” through established DL CPNs (Miyata et al., 2001; Sakakibara et al., 2014). The dynamic expression of *Mllt11* during UL CPN development also supports its role as a critical regulator of UL migration. Interestingly, mutations in  $\alpha$ -tubulin have been shown to cause axonal trafficking defects that impair synaptic stability and function without impacting axonal degeneration or neuronal survival (Buscaglia et al., 2020). The interaction of *Mllt11* with microtubules could therefore provide a mechanistic explanation for the impaired migration and reduced CPN dendritic complexity seen in *Mllt11* mutants. Specifically, we showed that *Mllt11* associates with acetylated  $\alpha$ -tubulin in fetal brain lysates, suggesting that it may be required for the stabilization of the cytoskeleton in growing neurites, and account for the similarities between the *Mllt11* mutant phenotype with those targeting tubulin isoforms.

The inefficient extension of neurites may also be attributed to impaired trafficking of organelles and ribosomes for local protein synthesis, or vesicles carrying secreted cues and growth cone machinery to the axonal periphery (Kennedy and Ehlers, 2006; González et al., 2016). Specifically, a potential *Mllt11* interactor Myosin 10 (Table 1) is known to regulate radial migration of CPNs through its effect on the localization of N-cadherin (Lai et

al., 2015), and has been implicated in tumor invasion by regulating process extension (Ropars et al., 2016). It is tempting to speculate that altered neuronal trafficking may underlie morphologic and transcriptional deficits of *Mllt11* mutant CPNs. Loss of *Mllt11* from the superficial cortex altered levels of UL2/3-specific transcription factors *Satb2* and *CDP/Cux1*, which function in establishment and maintenance of the CC as well as mature arborescent neuronal morphology and somal packing (Alcamo et al., 2008; Cubelos et al., 2015; Rodríguez-Tornos et al., 2016; He et al., 2021). Importantly, the loss of layer-specific morphology and identity has been demonstrated in postmortem brains from autistic humans (Casanova et al., 2013; Stoner et al., 2014; Fujimoto et al., 2021). These clinical data are reminiscent of the severe dysplasia in the cortex of our conditional *Mllt11* mutants, revealed by the Golgi staining method. It is presently unclear whether the loss of UL-specific gene expression we observed in our *Mllt11* mutants, and tubulinopathies more generally, is primarily because of cytoskeletal dysregulation, or other uncharacterized gene expression pathways functioning downstream of *Mllt11*. Some neuronal subtypes exhibit altered expression of subpopulation-specific markers when cytoskeletal regulation is altered such that connections to target regions cannot be established (Hippenmeyer et al., 2005), implying that there may be uncharacterized feedback mechanisms between establishment of connectivity and maintenance of expression of CPN subtype-specific transcription factors.

Other potential roles for *Mllt11* may depend on binding to chaperon protein HSPa8 and regulating protein export from the nucleus required for protein degradation (Li et al., 2014). Yet another possible function for *Mllt11* may include regulating the Wnt signaling cascade via T cell factor 7, which in turn regulates CD44 to promote cell migration and metastasis (Park et al., 2015; Li et al., 2018). As ours is the first study to explore *Mllt11* function in the developing brain, additional studies are needed to determine whether *Mllt11* could be exerting its effect on transcriptional regulation directly or indirectly via cytoskeletal interactions and intracellular trafficking, or both.

In light of this, we showed that the overexpression of *Mllt11* promoted migration into the CP, consistent with a cytoskeletal regulatory function. This finding is also consistent with *in vitro* studies, which showed that the overexpression of *Mllt11* in cancer stem cell lines promotes proliferation and invasiveness (Tse et al., 2017). It is possible that *Mllt11*-dependent cytoskeleton reorganization may favor symmetric divisions of organelles, nuclear components, and polarity protein complexes, therefore enhancing invasiveness of cells (Nance and Zallen, 2011; Piroli et al., 2019). On the other hand, the transcriptional regulation of *Mllt11* by REST has been associated with promoting neuronal differentiation, with high REST and low *Mllt11* expression in undifferentiated neuronal tissue, and increasing *Mllt11* levels correlated with decreased REST activity during terminal neuronal differentiation (Hu et al., 2015). These previously published findings, in conjunction with the complexity of the *Mllt11* mutant phenotype we reported here, imply that there are potentially two discrete pathways through which *Mllt11* regulates neuronal development: a cytoskeletal regulatory mechanism, and a transcriptional regulatory mechanism.

Much of what is known about *Mllt11* has been discerned from overexpression studies in immortalized cell lines and oncogenic clinical case studies, revealing pathogenic roles in cell process extension, invasiveness, and secretion of factors that promote efficient cellular motility (Lin et al., 2004; Tse et al., 2004; Li et al., 2006; Chang et al., 2008; Tiberio et al., 2017; Park et al.,

2019). Oncogenesis and neurogenesis share commonalities at the level of cytoskeletal regulation of somatic and nuclear morphology, as well as extension of and trafficking along cytoplasmic processes, allowing for invasion of and migration through tissues. However, it is important to make the distinction between pathologic studies and our current findings on the role of Mllt11. Until the current study, the physiological role for Mllt11 was unclear. In all the published *in vitro* and oncogenic case studies, Mllt11 is aberrantly overexpressed in non-neuronal tissues, either by itself or as a fusion with the chromatin remodeling protein Mll. We previously reported that Mllt11 protein and mRNA was exclusively localized to the developing CNS, and not in any other tissues (Yamada et al., 2014). The expression pattern of  $\beta$ -gal in the targeted *Mllt11* allele confirmed that it is normally expressed only within the developing CNS, with the highest levels reflecting UL cortical neurogenesis. Consistent with this expression profile, we now show that Mllt11 is required for proper migration but not neurogenesis of UL CPNs. Furthermore, we also revealed that Mllt11 regulates neurite outgrowth and the maintenance of UL gene expression programs. The loss of *Mllt11* led to a reduction of interhemispheric connectivity *via* reduced crossing callosal fibers. We also characterized a severe dysplasia of CPNs in *Mllt11* cKO mutant neonatal brains; a phenotype found in severe neurodevelopmental disorders such as ASD and Fragile X-associated tremor ataxia syndrome with which Mllt11 dysregulation has been associated (Xu et al., 2016; Drozd et al., 2019). Finally, we provide a possible mechanism of action for Mllt11 to link these phenotypes via its association with microtubules.

In summary, we investigated the role of Mllt11 in development of UL CPNs using a genetic KO and labeling strategy to target the superficial cortex. Numbers, laminar distribution, and morphology of UL CPNs were assessed over development. By combining *in vitro* and *in vivo* neurite outgrowth and morphology assays, we demonstrate that Mllt11 is required for neuronal invasion in the CP, formation of mature dendritic morphologies characteristic of UL CPNs, and the extension of axons across the CC. Mllt11 interacts with the microtubule cytoskeleton and likely exerts its effect by altering cytoskeletal organization during development. Whether the regulatory role of *Mllt11* is exerted through the stabilization of cytoskeletal architecture or by trafficking of cellular machinery along neurites will be the subject of future investigations.

## References

- Aboitiz F, Montiel J (2003) One hundred million years of interhemispheric communication: the history of the corpus callosum. *Braz J Med Biol Res* 36:409–420.
- Aiken J, Buscaglia G, Bates EA, Moore JK (2017) The  $\alpha$ -tubulin gene *TUBA1A* in brain development: a key ingredient in the neuronal isotype blend. *J Dev Biol* 5:8.
- Alcamo EA, Chirivella L, Dautzenberg M, Dobrova G, Fariñas I, Grosschedl R, McConnell SK (2008) *Satb2* regulates callosal projection neuron identity in the developing cerebral cortex. *Neuron* 57:364–377.
- Arlotta P, Molyneaux BJ, Chen J, Inoue J, Kominami R, Macklis JD (2005) Neuronal subtype-specific genes that control corticospinal motor neuron development *in vivo*. *Neuron* 45:207–221.
- Ayala R, Shu TZ, Tsai LH (2007) Trekking across the brain: the journey of neuronal migration. *Cell* 128:29–43.
- Bahi-Buisson N, Poirier K, Fourmiol F, Saillour Y, Valence S, Lebrun N, Hully M, Bianco CF, Boddaert N, Elie C, Lascelles K, Souville I, Beldjord C, Chelly J, Consortium LT; LIS-Tubulinopathies Consortium (2014) The wide spectrum of tubulinopathies: what are the key features for the diagnosis? *Brain* 137:1676–1700.
- Bellion A, Baudoin JP, Alvarez C, Bornens M, Métin C (2005) Nucleokinesis in tangentially migrating neurons comprises two alternating phases: forward migration of the Golgi/centrosome associated with centrosome splitting and myosin contraction at the rear. *J Neurosci* 25:5691–5699.
- Britanova O, de Juan Romero C, Cheung A, Kwan KY, Schwark M, Gyorgy A, Vogel T, Akopov S, Mitkovski M, Agoston D, Sestan N, Molnár Z, Tarabykin V (2008) *Satb2* is a postmitotic determinant for upper-layer neuron specification in the neocortex. *Neuron* 57:378–392.
- Brzustowicz LM, Hayter JE, Hodgkinson KA, Chow EWC, Bassett AS (2002) Fine mapping of the schizophrenia susceptibility locus on chromosome 1q22. *Hum Hered* 54:199–209.
- Brzustowicz LM, Simone J, Mohseni P, Hayter JE, Hodgkinson KA, Chow EWC, Bassett AS (2004) Linkage disequilibrium mapping of schizophrenia susceptibility to the CAPON region of chromosome 1q22. *Am J Hum Genet* 74:1057–1063.
- Buck KB, Zheng JQ (2002) Growth cone turning induced by direct local modification of microtubule dynamics. *J Neurosci* 22:9358–9367.
- Buscaglia G, Northington KR, Moore JK, Bates EA (2020) Reduced *TUBA1A* tubulin causes defects in trafficking and impaired adult motor behavior. *eNeuro* 7:ENEURO.0045-20.2020.
- Casanova MF, El-Baz AS, Kamat SS, Dombroski BA, Khalifa F, Elnakib A, Soliman A, Allison-McNutt A, Switala AE (2013) Focal cortical dysplasias in autism spectrum disorders. *Acta Neuropathol Commun* 1:67.
- Chai XJ, Förster E, Zhao ST, Bock HH, Frotscher M (2009) Reelin stabilizes the actin cytoskeleton of neuronal processes by inducing n-cofilin phosphorylation at serine3. *J Neurosci* 29:288–299.
- Chai XJ, Zhao ST, Fan L, Zhang W, Lu X, Shao H, Wang SB, Song LZ, Failla AV, Zobiak B, Mannherz HG, Frotscher M (2016) Reelin and cofilin cooperate during the migration of cortical neurons: a quantitative morphological analysis. *Development* 143:1029–1040.
- Chang XZ, Li DQ, Hou YF, Wu J, Lu JS, Di GH, Jin W, Ou ZL, Shen ZZ, Shao ZM (2008) Identification of the functional role of AF1Q in the progression of breast cancer. *Breast Cancer Res Treat* 111:65–78.
- Chen B, Wang SS, Hattox AM, Rayburn H, Nelson SB, McConnell SK (2008) The *Fezf2-Ctip2* genetic pathway regulates the fate choice of subcortical projection neurons in the developing cerebral cortex. *Proc Natl Acad Sci U S A* 105:11382–11387.
- Cubelos B, Sebastián-Serrano A, Kim SH, Redondo JM, Walsh C, Nieto M (2008a) *Cux-1* and *Cux-2* control the development of Reelin expressing cortical interneurons. *Dev Neurobiol* 68:917–925.
- Cubelos B, Sebastián-Serrano A, Kim S, Moreno-Ortiz C, Redondo JM, Walsh CA, Nieto M (2008b) *Cux-2* controls the proliferation of neuronal intermediate precursors of the cortical subventricular zone. *Cereb Cortex* 18:1758–1770.
- Cubelos B, Briz CG, Esteban-Ortega GM, Nieto M (2015) *Cux1* and *Cux2* selectively target basal and apical dendritic compartments of layer II-III cortical neurons. *Dev Neurobiol* 75:163–172.
- D'Amour KA, Gage FH (2003) Genetic and functional differences between multipotent neural and pluripotent embryonic stem cells. *Proc Natl Acad Sci U S A* 100:11866–11872.
- Dent EW, Kalil K (2001) Axon branching requires interactions between dynamic microtubules and actin filaments. *J Neurosci* 21:9757–9769.
- Drozd M, Delhaye S, Maurin T, Castagnola S, Grossi M, Brau F, Jarjat M, Willemsen R, Capovilla M, Hukema RK, Lalli E, Bardoni B (2019) Reduction of *Fmr1* mRNA levels rescues pathological features in cortical neurons in a model of FXTAS. *Mol Ther Nucleic Acids* 18:546–553.
- Ellis P, Fagan BM, Magness ST, Hutton S, Taranova O, Hayashi S, McMahon A, Rao M, Pevny L (2004) SOX2, a persistent marker for multipotential neural stem cells derived from embryonic stem cells, the embryo or the adult. *Dev Neurosci* 26:148–165.
- Fame RM, MacDonald JL, Macklis JD (2011) Development specification, and diversity of callosal projection neurons. *Trends Neurosci* 34:41–50.
- Frotscher M (1998) Cajal-Retzius cells, Reelin, and the formation of layers. *Curr Opin Neurobiol* 8:570–575.
- Fujimoto A, Enoki H, Niimi K, Nozaki T, Baba S, Shibamoto I, Otsuki Y, Oanishi T (2021) Epilepsy in patients with focal cortical dysplasia may be associated with autism spectrum disorder. *Epilepsy Behav* 120:107990.
- Gil-Sanz C, Franco SJ, Martínez-Garay I, Espinosa A, Harkins-Perry S, Müller U (2013) Cajal-Retzius cells instruct neuronal migration by coincidence signaling between secreted and contact-dependent guidance cues. *Neuron* 79:461–477.
- Gil-Sanz C, Espinosa A, Fregoso SP, Bluske KK, Cunningham CL, Martínez-Garay I, Zeng HK, Franco SJ, Müller U (2015) Lineage tracing using *Cux2-Cre* and *Cux2-CreERT2* mice. *Neuron* 86:1091–1099.



- Go CD, Knight JDR, Rajasekharan A, Rathod B, Hesketh GG, Abe KT, Youn JY, Samavarchi-Tehrani P, Zhang H, Zhu LY, Popiel E, Lambert JP, Coyaud É, Cheung SWT, Rajendran D, Wong CJ, Antonicka H, Pelletier L, Palazzo AF, Shoubhrie EA, et al. (2021) A proximity-dependent biotinylation map of a human cell. *Nature* 595:120–124.
- González C, Cánovas J, Fresno J, Couve E, Court FA, Couve A (2016) Axons provide the secretory machinery for trafficking of voltage-gated sodium channels in peripheral nerve. *Proc Natl Acad Sci U S A* 113:1823–1828.
- Götz M, Stoykova A, Gruss P (1998) Pax6 controls radial glia differentiation in the cerebral cortex. *Neuron* 21:1031–1044.
- He CH, Zhang L, Song NN, Mei WY, Chen JY, Hu L, Zhang Q, Wang YB, Ding YQ (2021) Satb2 regulates EphA7 to control soma spacing and self-avoidance of cortical pyramidal neurons. *Cereb Cortex*. Advance online publication. Retrieved Sep 21, 2021. doi:10.1093/cercor/bhab321.
- Hevner RF, Shi LM, Justice N, Hsueh YP, Sheng M, Smiga S, Bulfone A, Goffinet AM, Campagnoni AT, Rubenstein JLR (2001) Tbr1 regulates differentiation of the preplate and layer 6. *Neuron* 29:353–366.
- Hippenmeyer S, Vrieseling E, Sigrist M, Portmann T, Laengle C, Ladle DR, Arber S (2005) A developmental switch in the response of DRG neurons to ETS transcription factor signaling. *PLoS Biol* 3:e159.
- Hirokawa N, Takemura R (2004) Molecular motors in neuronal development, intracellular transport and diseases. *Curr Opin Neurobiol* 14:564–573.
- Hirota Y, Nakajima K (2017) Control of neuronal migration and aggregation by reelin signaling in the developing cerebral cortex. *Front Cell Dev Biol* 5:40.
- Hisaoka T, Nakamura Y, Senba E, Morikawa Y (2010) The forkhead transcription factors, Foxp1 and Foxp2, identify different subpopulations of projection neurons in the mouse cerebral cortex. *Neuroscience* 166:551–563.
- Hu YY, Sun QW, Zhang C, Sha QQ, Sun XL (2015) RE1 silencing transcription factor (REST) negatively regulates ALL1-fused from chromosome 1q (AF1q) gene transcription. *Bmc Mol Biol* 16:15.
- Iulianella A, Sharma M, Durnin M, Vanden Heuvel GB, Trainor PA (2008) Cux2 (Cutl2) integrates neural progenitor development with cell-cycle progression during spinal cord neurogenesis. *Development* 135:729–741.
- Keays DA, Tian G, Poirier K, Huang GJ, Siebold C, Cleak J, Oliver PL, Fray M, Harvey RJ, Molnár Z, Piñon MC, Dear N, Valdar W, Brown SDM, Davies KE, Rawlins JNP, Cowan NJ, Nolan P, Chelly J, Flint J (2007) Mutations in alpha-tubulin cause abnormal neuronal migration in mice and lissencephaly in humans. *Cell* 128:45–57.
- Kennedy MJ, Ehlers MD (2006) Organelles and trafficking machinery for postsynaptic plasticity. *Annu Rev Neurosci* 29:325–362.
- Kumamoto T, Toma K, Gunadi, McKenna WL, Kasukawa T, Katzman S, Chen B, Hanashima C (2013) Foxg1 coordinates the switch from nonradially to radially migrating glutamatergic subtypes in the neocortex through spatiotemporal repression. *Cell Rep* 3:931–945.
- Lai MM, Guo Y, Ma J, Yu HL, Zhao DD, Fan WQ, Ju XD, Sheikh MA, Malik YS, Xiong WC, Guo WX, Zhu XJ (2015) Myosin X regulates neuronal radial migration through interacting with N-cadherin. *Front Cell Neurosci* 9:326.
- Lawson ID, Krebs DL, Linossi EM, Zhang JG, McLennan TJ, Collin C, Mcrae HM, Kolesnik TB, Koh K, Britto JM, Kueh AJ, Sheikh BN, El-Saafin F, Nicola NA, Tan SS, Babon JJ, Nicholson SE, Alexander WS, Thomas T, Voss AK (2017) Cortical layer inversion and deregulation of reelin signaling in the absence of SOCS6 and SOCS7. *Cereb Cortex* 27:576–588.
- Lee H, Engel U, Rusch J, Scherrer S, Sheard K, Van Vactor D (2004) The microtubule plus end tracking protein orbit/MAST/CLASP acts downstream of the tyrosine kinase Abl in mediating axon guidance. *Neuron* 42:913–926.
- Leone DP, Heavner WE, Ferenczi EA, Dobreva G, Huguenard JR, Grosschedl R, McConnell SK (2015) Satb2 regulates the differentiation of both callosal and subcerebral projection neurons in the developing cerebral cortex. *Cereb Cortex* 25:3406–3419.
- Li DQ, Hou YF, Wu J, Chen Y, Lu JS, Di GH, Ou ZL, Shen ZZ, Ding J, Shao ZM (2006) Gene expression profile analysis of an isogenic tumour metastasis model reveals a functional role for oncogene AF1Q in breast cancer metastasis. *Eur J Cancer* 42:3274–3286.
- Li L, Jayabal S, Ghorbani M, Legault LM, McGraw S, Watt AJ, Yang XJ (2019) ATAT1 regulates forebrain development and stress-induced tubulin hyperacetylation. *Cell Mol Life Sci* 76:3621–3640.
- Li P, Ji M, Lu F, Zhang J, Li H, Cui T, Li Wang X, Tang D, Ji C (2014) Degradation of AF1Q by chaperone-mediated autophagy. *Exp Cell Res* 327:48–56.
- Li W, Ji M, Lu F, Pang Y, Dong X, Zhang J, Li P, Ye J, Zang S, Ma D, Ji C (2018) Novel AF1Q/MLLT11 favorably affects imatinib resistance and cell survival in chronic myeloid leukemia. *Cell Death Dis* 9:855.
- Lin HJ, Shaffer KM, Sun ZR, Jay G, He WW, Ma W (2004) AF1q, a differentially expressed gene during neuronal differentiation, transforms HEK cells into neuron-like cells. *Brain Res Mol Brain Res* 131:126–130.
- Lin S, Smith GM (2015) Acetylation as a mechanism that regulates axonal regeneration. *Neural Regen Res* 10:1034–1036.
- Lopez-Bendito G, Molnar Z (2003) Thalamocortical development: How are we going to get there? (vol 4, pg 276, 2003). *Nat Rev Neurosci* 4:422.
- Marín O, Rubenstein JLR (2003) Cell migration in the forebrain. *Annu Rev Neurosci* 26:441–483.
- Mensen VT, Wierenga LM, van Dijk S, Rijks Y, Oranje B, Mandl RCW, Durston S (2017) Development of cortical thickness and surface area in autism spectrum disorder. *Neuroimage Clin* 13:215–222.
- Miyata T, Kawaguchi A, Okano H, Ogawa M (2001) Asymmetric inheritance of radial glial fibers by cortical neurons. *Neuron* 31:727–741.
- Moffat JJ, Ka MH, Jung EM, Kim WY (2015) Genes and brain malformations associated with abnormal neuron positioning. *Mol Brain* 8:72.
- Moon HM, Wynshaw-Boris A (2013) Cytoskeleton in action: lissencephaly, a neuronal migration disorder. *Wiley Interdiscip Rev Dev Biol* 2:229–245.
- Nadarajah B, Brunstrom JE, Grutzendler J, Wong ROL, Pearlman AL (2001) Two modes of radial migration in early development of the cerebral cortex. *Nat Neurosci* 4:143–150.
- Nance J, Zallen JA (2011) Elaborating polarity: PAR proteins and the cytoskeleton. *Development* 138:799–809.
- Nieto M, Monuki ES, Tang H, Imitola J, Haubst N, Khoury SJ, Cunningham J, Gotz M, Walsh CA (2004) Expression of Cux-1 and Cux-2 in the subventricular zone and upper layers II-IV of the cerebral cortex. *J Comp Neurol* 479:168–180.
- Park J, Schleder M, Schreiber M, Ice R, Merkel O, Bilban M, Hofbauer S, Kim S, Addison J, Zou J, Ji C, Bunting ST, Wang Z, Shoham M, Huang G, Bago-Horvath Z, Gibson LF, Rojanasakul Y, Remick S, Ivanov A, et al. (2015) AF1q is a novel TCF7 co-factor which activates CD44 and promotes breast cancer metastasis. *Oncotarget* 6:20697–20710.
- Park J, Hwang JY, Thore A, Kim S, Togano T, Hagiwara S, Park JW, Tse W (2019) AF1q inhibited T cell attachment to breast cancer cell by attenuating intracellular adhesion molecule-1 expression. *J Cancer Metastasis Treat* 5:17.
- Pirollo ME, Blanchette JO, Jabbarzadeh E (2019) Polarity as a physiological modulator of cell function. *Front Biosci (Landmark Ed)* 24:451–462.
- Reyes NSD, Mederos S, Varela I, Weiss LA, Perea G, Galazo MJ, Nieto M (2019) Transient callosal projections of L4 neurons are eliminated for the acquisition of local connectivity. *Nat Commun* 10:4549.
- Rodríguez-Tornos FM, Briz CG, Weiss LA, Sebastián-Serrano A, Ares S, Navarrete M, Frangeul L, Galazo M, Jabaudon D, Esteban JA, Nieto M (2016) Cux1 enables interhemispheric connections of layer II/III neurons by regulating Kv1-dependent firing. *Neuron* 89:494–506.
- Ropars V, Yang ZH, Isabet T, Blanc F, Zhou KF, Lin TM, Liu XY, Hissier P, Samazan F, Amigues B, Yang ED, Park H, Pylypenko O, Cecchini M, Sindelar CV, Sweeney HL, Houdusse A (2016) The myosin X motor is optimized for movement on actin bundles. *Nat Commun* 7:12456.
- Saito T (2006) In vivo electroporation in the embryonic mouse central nervous system. *Nat Protoc* 1:1552–1558.
- Sakakibara A, Sato T, Ando R, Noguchi N, Masaoka M, Miyata T (2014) Dynamics of centrosome translocation and microtubule organization in neocortical neurons during distinct modes of polarization. *Cereb Cortex* 24:1301–1310.
- Schindelin J, Arganda-Carreras I, Frise E, Kaynig V, Longair M, Pietzsch T, Preibisch S, Rueden C, Saalfeld S, Schmid B, Tinevez JY, White DJ, Hartenstein V, Eliceiri K, Tomancak P, Cardona A (2012) Fiji: an open-source platform for biological-image analysis. *Nat Methods* 9:676–682.
- Stoner R, Chow ML, Boyle MP, Sunkin SM, Mouton PR, Roy S, Wynshaw-Boris A, Colamarino SA, Lein ES, Courchesne E (2014) Patches of disorganization in the neocortex of children with autism. *N Engl J Med* 370:1209–1219.
- Su YS, Ding WH, Xing MJ, Qi DK, Li ZZ, Cui DH (2017) The interaction of TXNIP and AF1q genes increases the susceptibility of schizophrenia. *Mol Neurobiol* 54:4806–4812.

- Sudo H, Baas PW (2010) Acetylation of microtubules influences their sensitivity to severing by katanin in neurons and fibroblasts. *J Neurosci* 30:7215–7226.
- Thomson AM (2010) Neocortical layer 6, a review. *Front Neuroanat* 4:13.
- Tiberio P, Lozaneanu L, Angeloni V, Cavadini E, Pinciroli P, Callari M, Carcangiu ML, Lorusso D, Raspagliesi F, Pala V, Daidone MG, Appierto V (2017) Involvement of AF1q/MLLT11 in the progression of ovarian cancer. *Oncotarget* 8:23246–23264.
- Toma K, Kumamoto T, Hanashima C (2014) The timing of upper-layer neurogenesis is conferred by sequential derepression and negative feedback from deep-layer neurons. *J Neurosci* 34:13259–13276.
- Tsai JW, Bremner KH, Vallee RB (2007) Dual subcellular roles for LIS1 and dynein in radial neuronal migration in live brain tissue. *Nat Neurosci* 10:970–979.
- Tse CO, Kim S, Park J (2017) Activation of Wnt signaling pathway by AF1q enriches stem-like population and enhance mammosphere formation of breast cells. *Biochem Biophys Res Commun* 484:884–889.
- Tse W, Zhu WM, Chen HS, Cohen A (1995) A novel gene, Af1q, fused to Mll in T(1-11)(Q21-Q23), is specifically expressed in leukemic and immature hematopoietic-cells. *Blood* 85:650–656.
- Tse W, Meshinchi S, Alonzo TA, Stirewalt DL, Gerbing RB, Woods WG, Appelbaum FR, Radich JP (2004) Elevated expression of the AF1q gene, an MLL fusion partner, is an independent adverse prognostic factor in pediatric acute myeloid leukemia. *Blood* 104:3058–3063.
- Tueting P, Costa E, Dwivedi Y, Guidotti A, Impagnatiello F, Manev R, Pesold C (1999) The phenotypic characteristics of heterozygous reeler mouse. *Neuroreport* 10:1329–1334.
- Wei D, Gao NN, Li L, Zhu JX, Diao L, Huang JS, Han QJ, Wang SG, Xue HQ, Wang Q, Wu QF, Zhang X, Bao L (2018)  $\alpha$ -Tubulin acetylation restricts axon overbranching by dampening microtubule plus-end dynamics in neurons. *Cereb Cortex* 28:3332–3346.
- Weng LQ, Zhang WB, Ye Y, Yin PP, Yuan J, Wang XX, Kang L, Jiang SS, You JY, Wu J, Gong H, Ge JB, Zou YZ (2014) Aliskiren ameliorates pressure overload-induced heart hypertrophy and fibrosis in mice. *Acta Pharmacol Sin* 35:1005–1014.
- Xu Q, Goldstein J, Wang P, Gadi IK, Labreche H, Rehder C, Wang WP, McConkie A, Xu X, Jiang YH (2016) Chromosomal microarray analysis in clinical evaluation of neurodevelopmental disorders-reporting a novel deletion of SETDB1 and illustration of counseling challenge. *Pediatr Res* 80:371–381.
- Yamada M, Clark J, Iulianella A (2014) MLLT11/AF1q is differentially expressed in maturing neurons during development. *Gene Expr Patterns* 15:80–87.
- Yamada M, Clark J, McClelland C, Capaldo E, Ray A, Iulianella A (2015) Cux2 activity defines a subpopulation of perinatal neurogenic progenitors in the hippocampus. *Hippocampus* 25:253–267.
- Zhou FQ, Zhou J, Dedhar S, Wu YH, Snider WD (2004) NGF-induced axon growth is mediated by localized inactivation of GSK-3 $\beta$  and functions of the microtubule plus end binding protein APC. *Neuron* 42:897–912.
- Zimmer C, Tiveron MC, Bodmer R, Cremer H (2004) Dynamics of Cux2 expression suggests that an early pool of SVZ precursors is fated to become upper cortical layer neurons. *Cereb Cortex* 14:1408–1420.